Marius Pytten

Accuracy assessment of the Schmidt hammer exposure-age dating method and comparative analysis of temporal distributions of large rock slope failures

In the western gneiss region, Norway

NTNU
Kunnskap for en bedre verden

Marius Pytten

Accuracy assessment of the Schmidt hammer exposure-age dating method and comparative analysis of temporal distributions of large rock slope failures

In the western gneiss region, Norway

NTNU
Kunnskap for en bedre verden

Abstract

This Master's thesis investigates on the application and accuracy of the Schmidt hammer exposure age dating method on large rock slope failure deposits in the western gneiss region in Norway. The unique situation of having 20 terrestrial cosmogenic nuclide-dated, ^{14}C-dated and historical documented rock slope failures in the region were used to test the method on multiple calibration sites. This approach is different to former research because it includes several deposits with a wide range of ages instead of only one young and one old deposit as calibration sites.

This study indicates that although there is an inversely proportional correlation between exposure time and surface hardness, there is an enormous spread of rebound values within each deposit, often not replicating a normal distribution. This large spread of rebound values is attributed to surface roughness of boulders resulting from rock slope failure, weathering prior to the failure event and mineral heterogeneity. These influences cause the Schmidt hammer exposure age dating method to have a low accuracy and reliability on rock slope failures in gneissic lithology. The development of a new method that is statistically significant failed as the proposed method gave too large uncertainties to use for any interpretation.

The temporal distribution of rock slope failures in the western gneiss region was compared to the timing of glacial retreat in the valleys. Two clusters were identified: one near the time of deglaciation and another during the Holocene thermal maximum. A warmer climate, retreating glaciers, and seismic triggering due to rapid isostatic rebound are expected to contribute to a higher frequency of large rock slope failures during these periods.

Sammendrag

Denne masteroppgaven undersøker anvendelsen og nøyaktigheten av Schmidt hammer dateringsmetoden på fjellskredavsetninger i den vestre gneisregionen i Norge. Oppgaven utnytter at det i studieområdet eksisterer 20 avsetninger med en allerede kjent alder, funnet ved hjelp av terrestrisk kosmogenisk nuklide-datering, ^{14}C-datering og i historiske arkiver over skredhendelser i historisk tid, til å teste metoden på et stort antall kalibreringsområder. Denne tilnærmingen skiller seg ut fra tidligere forskning fordi den inkluderer flere skredavsetninger med et bredt spekter av aldre, i stedet for kun én ung og én gammel avsetning.

Denne studien indikerer at selv om det er en omvendt proporsjonal korrelasjon mellom eksponeringstid og overflatehardhet, er det en enorm spredning av R-verdier for hver respektive skredavsetning. Disse er i tillegg ofte ikke normalfordelte. Denne store spredningen av R-verdier tilskrives overflateruheten til blokkene, forvitring av det ustabile partiet før skredhendelsen og mineralheterogenitet. Disse påvirkningene fører til at Schmidt hammer dateringsmetoden har lav nøyaktighet og pålitelighet for skred i områder med gneisholdige bergarter. Utviklingen av en ny metode som er statistisk signifikant mislyktes, da den foreslåtte metoden ga for store usikkerheter til å kunne brukes til tolkning.

Den tidsmessige fordelingen av fjellskred i den vestre gneisregionen ble sammenlignet med tidspunktene for isens tilbaketrekning i dalene. To perioder med økt skredaktivitet ble identifisert: én nær tidspunktet for deglasiasjon og en annen under det termale maksimum i Holocen. Et varmere klima, tilbaketrekning av isbreer og seismisk aktivitet på grunn av rask isostatisk landhevning forventes å ha bidratt til en høyere frekvens av fjellskred i disse periodene.

Preface

This Master's thesis is the conclusion of five years of geology studies. A lot of people have contributed to a memorable year and I am incredibly grateful for their contributions.

First of all I would like to thank my great supervisors Reginald L. Hermanns and François Noël. Their technical expertise is unquestionable, and I have very much enjoyed our time together.

I would also like to thank my field assistants Jonas V. Andreassen and Oda K. Vogt. Thank you for wonderful days of hiking and hammering rocks. A thanks to Pierrick Nicolet for guidance and proposals on statistical analysis, to Ernst Å. Pytten for proofreading and to my personal IT-support Ingri H. Nygaardsmoen.

Through three weeks of field work I have had the pleasure of meeting and getting to know local inhabitants of Romsdalen, Sunndalen, Eikesdalen and surrounding areas. I was met by an incredible hospitality and friendliness. Whether it was help with accomodation, advice on how to get to locations or access to remote and bumpy gravel roads in the mountains, I was never met by any hesitation. A special thanks to Perly, Bjørn and Amanda Eikås for lodging, advice and interest in my project.

In the end I would like to thank all my classmates for an amazing time together as students and for keeping my motivation up during though periods of my work.

Trondheim, May 2024

Marius Pytten

Contents

List of Figures

List of Tables

1   Introduction

Temporal dating of geological structures is a critical component of understanding Earth's dynamic history and changes over time. Large rock slope failures contribute to rapid changes of the landscape and traces of these massive events are visible across the steep valleys carved by the ice in western Norway. Historical records in this region document several catastrophic events, including the Tjellefonna rock avalanche in 1756, the Tafjord disaster in 1934, and the Loen events in 1905, 1936, and 1950 (Furseth, 2006; Sandøy et al., 2016). These events collectively caused extensive damage and resulted in the loss of 267 human lives.

To study the temporal distribution of these occurrences has a high importance to understand their conditioning factors, triggers and recurrence intervals (Blikra et al., 2006; Hermanns et al., 2006). This contributes to an enhanced predictability and understanding of necessary mitigation measures to ensure that the outcome of an event is not as catastrophic as some of the prior incidents.

The study area is located in the western gneiss region in the county of Møre og Romsdal and extends over multiple formerly glaciated valleys. The last glaciers retreated during and after the Younger Dryas period 12 800 to 11 600 (Hughes et al., 2015; Romundset et al., 2023). The glaciers and their carving of the landscape could have an influence on the rock slope instabilities and rock slope failures in the study area. Removal of glacial support contributes to destabilization and may cause rapid collapse of rock slopes (Kos et al., 2016). Permafrost degradation is also highly influential to the destabilization of rock slopes (Hilger et al., 2021), and an increased rock slope failure activity is detected during the Holocene thermal maximum 8000 - 5000 years ago (Marr et al., 2019).

Regularly applied methods for determination of the temporal occurrence of geological processes include Terrestial cosmogenic nuclide dating (TCN) and Radiocarbon dating (Walker, 2005).

Another method, that has seen an increasing popularity the last 20 years, is the Schmidt Hammer dating method (SHD). The Schmidt Hammer was initially an

invention to test the hardness and hence the quality of concrete (Aydin and Basu, 2005). In the last 30 years the hammer has become a more integrated tool in the geological community, used to date various kinds of exposed surfaces.

The SHD method is based on quantification of the degree of weathering for a surface, where linear regression between two control surfaces is used to estimate the exposure time of a surface where the age is unknown (Matthews and Owen, 2010). Some advantages is the easy and fast applicability and low cost, which has led to a increasing popularity of the method (Basu and Aydin, 2004; Ffoulkes and Harrison, 2014).

The method has through recent advances been called a high-precision dating technique (Shakesby et al., 2006; Matthews and Owen, 2010; Matthews and Winkler, 2011; Matthews and McEwen, 2013; Marr et al., 2019) and Wilson et al. (2019) suggest it is of comparable accuracy and may have improved precision over ages estimated by TCN-dating. As the reliance on this method grows, it becomes crucial to critically examine its efficacy and question whether it lives up to the claims of precision and accuracy that have been made.

Shakesby et al. (2011) proves how well the method works on granite surfaces by comparing the method to different surfaces with a great range of already known ages. A similar test is still to be performed in gneiss, the most common lithology to apply the method to for investigations in Norway.

1.1 Research objectives

The research objectives of this Master's thesis is to:

1. Investigate the accuracy of the Schmidt hammer dating method for large rock slope failures in Norwegian gneiss, to determine its applicability as a tool for exposure age estimation.

2. Compare the temporal distribution of large rock slope failures and timing of deglaciation of valleys in western Norway, to contribute to an understanding of their correlation.

To fulfill these objectives extensive field work in the western gneiss region in Norway was performed. Schmidt hammer measurements on multiple rock slope failure deposits were collected. The area is well investigated and the ages of 20 of the deposits is already known through TCN-dating, radiocarbon dating and documentations of historical events. The range of these ages makes it possible to analyse if there are any differences between theoretical expectations and practical outcomes. Dating of 7 deposits with unknown age where also attempted in accordance to the results of the analysis.

The temporal distribution attained from the SHD-dating method and former investigations were compared to the Dated-1 database (Hughes et al., 2015), which provides information on the timing of deglaciation in Norway.

2 Theory

2.1 Rock weathering

Weathering is a process occurring in exposed rock faces over time. Bland and Rolls (2016) describes how weathering includes multiple processes that cooperate to change the properties of the material. Physical weathering occurs due to mechanical processes such as freeze-thaw cycles, where water seeps into cracks in the rock where it freezes and expands, causing the rock to break apart over time. Similarly, abrasion from wind-blown sand and water impacting the rock can contribute to a breakdown into smaller particles. Chemical weathering is changing the minerals through chemical reactions with water and air. For example, feldspar minerals can undergo hydrolysis, where water reacts with the mineral to form clay minerals and dissolved ions (Bland and Rolls, 2016). This process weakens the structure of the rock. Biological weathering is caused by the action of organisms. Plant roots creates cracks in the rock, while organic acids released by microbial activity can accelerate the chemical weathering processes (Bland and Rolls, 2016). These weathering processes contributes to weakening the rock surfaces over time.

2.2 Rock slope failures

Rock slope failure is an umbrella term which includes landslide processes involving rocks (Hermanns et al., 2022). It is a term that includes different kinds of failure and involves the whole process from prefailure deformation through the moment of failure to the post failure deformation. The term can subdivided into three different categories for rapid failures: rock fall, rock collapse and rock avalanche. Each is characterized through size, movement patterns and failure mechanisms (Dorren, 2003). A well-known characterization parameter is the Farbõrschung angle, also called the angle of reach (Figure 1). This angle is the angle between a line drawn from the top of the back scarp of the failure to the outermost point on the toe of the deposit and the horizontal.

Figure 1: A schematic drawing representing a rock avalanche with Farbõrschung (α), fall height (H) and run-out lenth (L). Modified from: Hermanns et al. (2022)

Rock fall is one of the most common modes of failure. It can be described as the sudden detachment and free fall of individual rock blocks or fragments. Rock falls typically occur on steep cliffs and rock faces. They are often triggered by weathering and frost-thaw activity, but may also occur due to factors such as seismic activity and human disturbance (Dorren, 2003). The rocks and fragments usually does not interact and behave individually. The volume is small, typically less than 10 000 m^3 while the Farbõrschung is often $> 32°$ and the H/L ratio > 0.625, but 5-28% of blocks may travel further at a lower angle (Evans and Hungr, 1993; Hermanns et al., 2022).

The second mode is rock collapse, which includes a larger and more coherent mass moving at the same time down the slope. It is still limited interactions between the rocks and both sliding, jumping and rolling occurs in the event (Hermanns et al., 2022). The lower limit is typically 10 000 m^3. Rock collapse have the potential to entail and move larger masses along the slope which may increase the total mass influenced by the event. The total mass may therefore be as large as 10 000 000 m^3, but there is not registered any rock collapse events where more than 100 000 m^3 is moving simultaneously. Also here the Farbõrschung is often $> 32°$ and the H/L ratio > 0.625 (Hermanns et al., 2022).

In the case of a total mass larger than 100 000 m^3 moving simultaneously it trans-

itions over to the last mode of failure: rock avalanches. Large rock avalanches inherit a different behaviour compared to the other processes as they involve massive volumes of rocks (Hilger et al., 2022). They are characterized by high energy and destructive forces. As these immense masses of rock detach from the mountainside, they undergo fragmentation and pulverization, transforming into a flowing mass that travels down the slope, despite the minimal presence of water within the rock mass. The sheer magnitude of energy involved in these sliding movements enables rock avalanches to travel several kilometers, in contrast to rock falls and and rock slides. Here the Farbõrschung is $< 32°$ and the H/L ratio < 0.625. The reason for this long travel distance is continuous interaction between the fragments in the process (Hermanns et al., 2022). Rock avalanches are a result of slow moving bodies of rock over a period of time accelerating due to crack propagation and breaking of rock bridges (Hilger et al., 2022). This implies that some rock faces are exposed to weathering prior to the event as the cracks develops over time.

Rock avalanches are usually well preserved and easy detectable features, as they inherit very large masses of massive rock. They are recognised by large volumes covering large areas, not only close to their source. One way to detect rock avalanches is by using a Digital Terrain Model (DTM). They can be recognised by large distinguishable rock features where the travel distance and deposit area is great compared to the source area.

2.3   Dating methods

To determine the timing of different rock slope failure events, a variety of methods may be applied. Some are related to the direct exposure and change by time of the rock surface itself, such as Schmidt hammer exposure age dating and Terrestrial cosmogenic nuclide dating (TCN), while some rely on organic material influenced by the rock slope failure event, such as radiocarbon dating.

2.3.1 TCN-dating

Terrestrial cosmogenic nuclide dating is a well established method for determination of the exposure age of a rock surface in Quaternary science (Walker, 2005). When high-energy cosmic rays enter the atmosphere they collide with nuclei. This process triggers high energy neutrons (and a small number of muons) which is sent towards the surface of the earth. When the neutrons hits an exposed surface, the nuclides in certain minerals are subject to a spallation process - a process where the nuclei is broken in smaller fragments and new nuclides are formed. The longer the time of exposure for the surface, the higher the concentration of the secondary formed nuclides. Hence a relation between age and concentration of certain nuclides can be established. One common nuclei to use is the ^{10}Be-isotope as demonstrated by Wilson et al. (2019).

2.3.2 Radiocarbon dating

Radiocarbon dating is also a method influenced by the collision of cosmic rays (Walker, 2005). When the neutrons produced by the cosmic rays interact with ^{14}N in the atmosphere, the ^{14}C-isotope is formed. This isotope is very rare in nature and only $1/10^{10}\%$ of all carbon appears in this form. Through , the ^{14}C is absorbed by plants during their lifetime, which again are eaten by animals. This way the ^{14}C exists in the food chain and are present in the tissues of living organisms. The global reservoir of ^{14}C is in an equilibrium, meaning that the amount of ^{14}C in the tissues of organisms stays at a fairly constant level.

When an organism dies, it no longer ingests new ^{14}C. As the ^{14}C is not a stable isotope, it decays to a stable form - ^{14}N. The decay follows a exponential curve. Therefore the percentage of decay at any moment in time is constant (Walker, 2005). Half-life of the isotope can be measured and therefore be related to the initial time of decay. This enables the possibility to calculate the time of death for an organism by measuring half-lives of the isotope.

Radiocarbon has also been applied to Quaternary geological dating (Matthews and

Winkler, 2010; Matthews et al., 2014; Matthews et al., 2019; Matthews et al., 2020b). As the rocks are non-organic they do not contain ^{14}C. The dating must therefore be performed on organic material influenced or related to the material of interest.

2.4 Statistical parameters

To analyze a collection of data, some statistical parameters are essential. The parameters applied to the data in this study and described in this chapter are adapted from Løvås (2018).

Average or the mean value is the is the typical value in a set of data. It is calculated by taking the sum of the data and dividing it by the number of measurements:

$$\bar{x} = \frac{x_1 + x_2 + \ldots + x_n}{n} \tag{1}$$

Where $x_1 + x_2 + \ldots + x_n$ are the individual values and n is the total number of values in the dataset.

The normal distribution or the Gaussian distribution is a continuous random variable where the data tends to cluster around the mean with symmetric tails extending equally in both directions (figure 2). The spread of the distribution is determined by the **standard deviation (σ)**, which is a measure of the amount of variation in a dataset. In a perfect normal distribution, 68% of the data falls within one standard deviation of the mean, 95% within two standard deviations, and 99% within three standard deviations. This is referred to as 1σ, 2σ and 3σ.

It is possible to work with data with a known standard deviation for the population which are studied. In this case this standard deviation can be used directly in the statistical analysis. In scientific work it is more common to work with a population or a set of data without a known standard deviation. In this case the estimated standard deviation of the sample (s) has to be calculated. This is an estimation of the average distance from the data points to the mean of the dataset and is
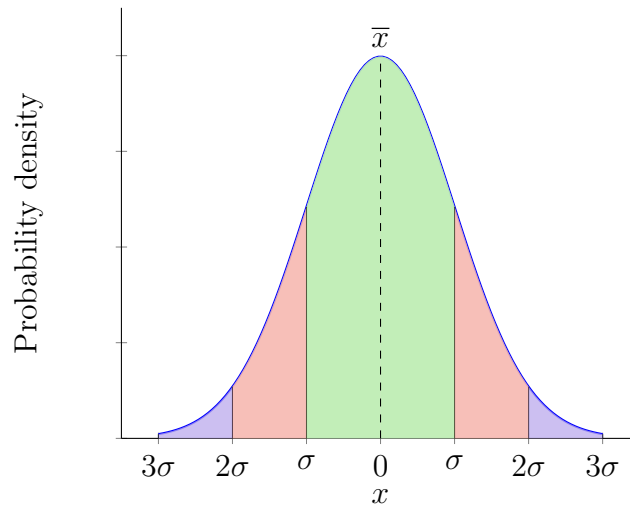
Figure 2: Normal distribution with the mean at the peak $(\bar{x})$ and regions representing each interval for one, two and three standard deviations.

calculated according to the formula:

$$s = \sqrt{\frac{\sum_{i=1}^{n}(x_i - \bar{x})^2}{n-1}} \qquad (2)$$

where x_i represents an individual data point.

A higher standard deviation indicates more variability in the data, while a lower standard deviation indicates that each data point is on average closer to the mean.

Standard error measures the variability of sample means around the mean for the dataset. It is calculated by dividing the standard deviation of the dataset by the square root of the number of measurements:

$$SE = \frac{s}{\sqrt{n}} \qquad (3)$$

Confidence intervals Confidence intervals provide a range of values where the true value has a certain probability to be within. In a normal distribution this probability, or level of confidence, is expressed in percentage or number of standard deviations(σ). Levels of confidence for 1σ, 2σ and 3σ are presented in figure 3.
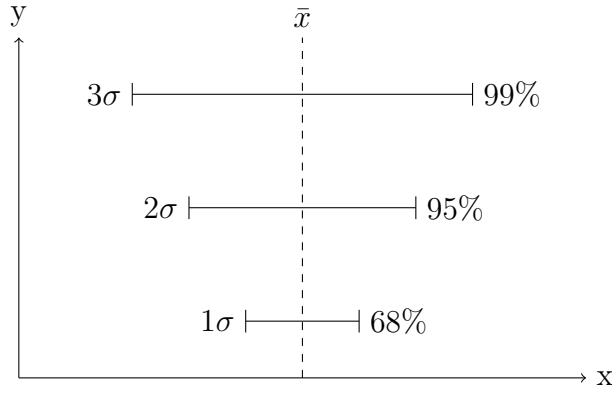
Figure 3: Representation of confidence intervals with different levels of confidence. The range of the intervals becomes smaller with lower confidence level.

The confidence intervals are calculated by adding and subtracting the margin of error from the sample mean estimate. The margin of error is determined by multiplying the standard error by a critical value (Table 1) from the standard normal distribution:

$$\mathrm{CI} = \bar{x} \pm Z \left(\frac{\sigma}{\sqrt{n}} \right) \tag{4}$$

where Z is the critical value according to the chosen level of confidence. The Z value for each level of confidence can be found in table 1.

Confidence Level (%)	σ	Z-value
68	1	1
95	2	1.96
99	3	2.58

Table 1: Z-values for different confidence levels.

If the standard deviation and hence the standard error is unknown, they have to be estimated according to the formula for the estimated standard deviation and the formula for the standard error. In this case the standard error has become stochastic

as it depends on the observed value of s. In this case another distribution is applied to the data, the **Student's t-distribution**. This distribution is dependent on the estimated standard deviation and the formula for the t-interval can be expressed as:

$$\text{CI} = \bar{x} \pm t \left(\frac{s}{\sqrt{n}} \right) \tag{5}$$

Some t-values for 100 degrees of freedom can be found in table 2.

Confidence Level (%)	Degrees of Freedom	T-value
68	100	1
95	100	1.98
99	100	2.63

Table 2: T-values for different confidence levels with 100 degrees of freedom.

Degrees of freedom is found by $n - 1$.

Student t-statistics differs from the normal distribution with a lower peak and a slightly wider spread of data. It is best suited for small population sizes and with $n > 30$, the t-value is getting close to the same as the Z-value for the normal distribution. This can be observed by comparing table 1 and 2.

Outliers are data points that deviate significantly from the rest of the data. They occur due to different reasons, such as measurement errors and natural variability. The mean value is highly affected by outliers as represented in figure 4.

The figure proves a high influence on the mean by a few outliers. Other statistical approaches may diminish these effects.
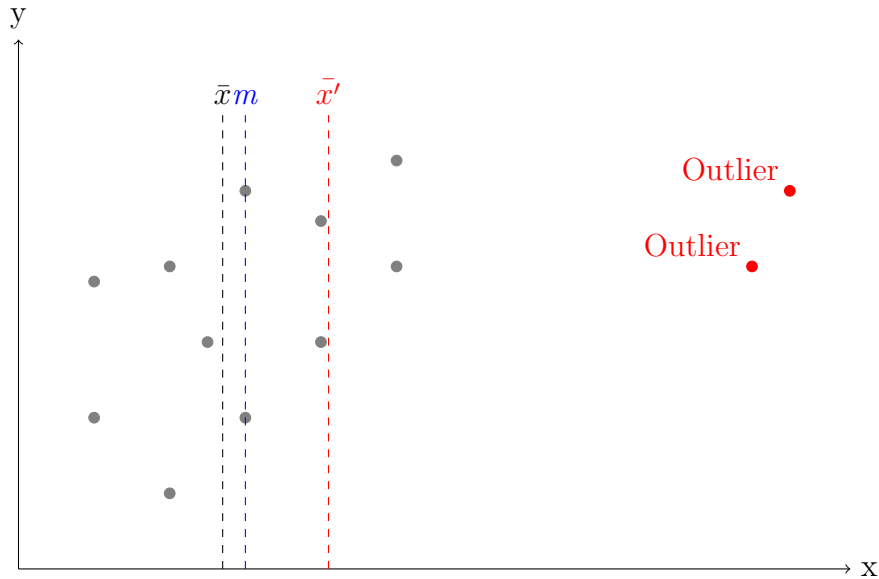
Figure 4: Representation of a set of data including two extreme values and the effect on the mean and the median. $\bar{x}$ and $\bar{x}'$ represents the average without and with the outliers accordingly, while m represents the median, including and excluding outliers where the position remains the same regardless of the outliers.

The **median** splits the dataset in two equal parts and the observation exactly in the middle is the median value. The value of each individual data point has in this way a smaller effect on the overall result. Therefore one or few extreme values has a smaller effect on the median as demonstrated in figure 4.

Percentiles is common to use to determine uncertainties for the median in a dataset. The median can be referred to as the 50th percentile, since 50% of the values are less or equal to it. In the same way we can also define the 25th percentile and 75th percentile, commonly known as **quartiles**. Figure 5 demonstrates how percentiles can be presented in a box plot.
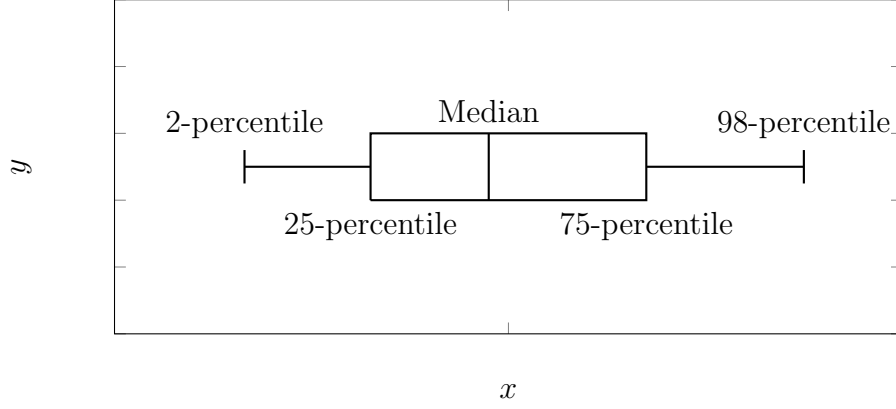
Figure 5: Box plot demonstrating median and 2nd, 98th, 25th and 75th quartiles. Max and min values or other quartiles could also be used for box plots.

Correlation is a statistical tool to determine how much two or more values are related to each other. One way of determining the correlation is by the **Kendall's** τ. This tool measures the correlation on a scale between -1 and 1, where -1 is a perfect negative correlation, 1 a perfect positive correlation and 0 shows no correlation between the data (Penna et al., 2023). It is calculated from:

$$\tau = \frac{C - D}{\sqrt{\left(\frac{n(n-1)}{2} - T_x\right)\left(\frac{n(n-1)}{2} - T_y\right)}} \tag{6}$$

where C represents the count of concordant pairs, while D is for the count of discordant pairs. Tx and Ty indicate the number of ties observed on the x and y variables. A concordant pair refers to a pair of data points (x1, y1) and (x2, y2) where either both x1 and y1 are greater than x2 and y2 respectively, or both x1 and y1 are less than x2 and y2 respectively. This definition is adapted from Agresti (2010).

The p-value is a value quantifying the statistical significance of the data. The lower the p-value, the less likely the data is to fulfill the null-hypothesis (Penna et al., 2023). The null-hypothesis is a statement that suggests there is no significance in the data being analyzed, and is normally rejected for p-values under 0.05.

To do a quantitative assessment to control if a set of data has a normal distribution, the **Shapiro-Wilk test** can be performed (King and Eckersley, 2019). The null hypothesis for this test is that the data is a normal distribution, while the alternative

hypothesis suggests that it is not. If the value from the test is less than 0.05, the null-hypothesis can be rejected with 95% confidence. The null-hypothesis can not be rejected if the value is above 0.05, and the data may be normal distributed (King and Eckersley, 2019).

2.5   The Schmidt hammer

The Schmidt Hammer is a simple tool developed to test the hardness and hence the quality of concrete (Proceq, 2002). It was later also introduced in rock mechanics to measure the hardness of rock surfaces. Its operation relies on a fundamental principle of physics: the rebound of a mass striking a surface is directly related to the surface's hardness.

The device consists of a spring-loaded hammer enclosed in a housing with a striking plunger at the end. When the plunger is pressed against the surface and released, the hammer strikes the surface, causing it to rebound. The rebound distance, which is shown on the device, is called the R-value. The R-value can be defined as:

$$R = (x_2/x_1) * 100 \tag{7}$$

where x_1 represents the starting point of the spring, when fully loaded ready for impact and x_2 represents the rebound distance. The value is expressed in percentage, giving an impression of how much of the energy is conserved and how much is transferred. The energy lost is transferred to sound and heat, and plastic deformation of the surface. The remaining energy is conserved and reflects the work done on the surface. A softer surface will require more work and give a longer penetration time, a smaller impulse, which will lead to a larger momentum change and therefore a lower energy return (Basu and Aydin, 2004).

The hardness of the surface influences the rebound distance: harder surfaces result in higher R-values, while softer surfaces yield smaller rebound distances and hence lower R-values. This relationship enables the possibility to quickly, while inducing limited damage, assess the concrete or rock surface hardness.
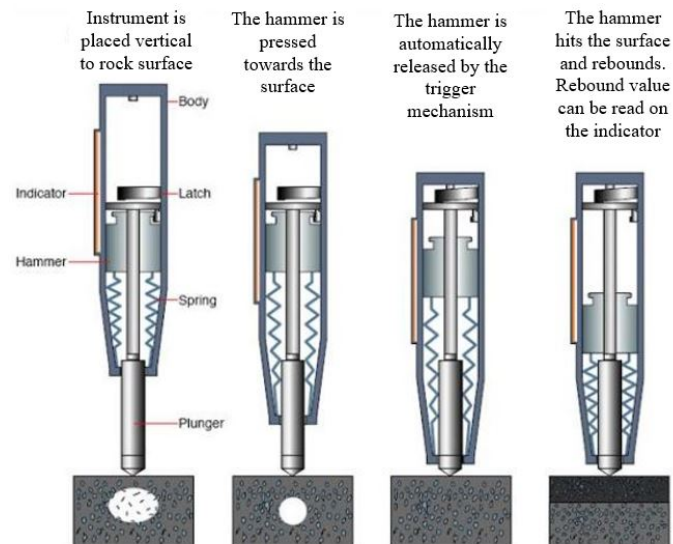
Figure 6: Illustration of the principles of the Schmidt hammer. The hammer is pressed on the test surface to maximum load where the plunger is automatically released. It rebounds from the surface with the R-value shown on the indicator. Modified from Castañeda et al. (2017)

2.5.1 Hammer type

Three different kinds of Schmidt hammer exists, whereas only two of them are suitable for testing of rocks (Goudie, 2006):

- The N hammer has a range from 20 to 250 MPa and gives an impact of 2.207 Nm. This is the hammer normally used in geological research as the hammer covers a wider range more suitable for rocks.

- The L hammer gives an impact of 0.735 and is therefore better suited for weak rocks which breaks more easily.

2.5.2 Angle calibration

In-situ testing may exhibit the challenge of different angles of the surfaces. When conducting Schmidt Hammer tests on non-horizontal surfaces, the angle of the surface relative to the vertical may affect the rebound distance. Gravity exert a down-

ward force on the mass of the hammer during the rebound phase, making the angle critical for the measured R-value.

To account for these gravitational influences and ensure accurate results, calibration of the Schmidt Hammer is necessary. It is suggested by Basu and Aydin (2004) to normalize for a horizontal impact on a vertical surface. Articles using the Schmidt hammer as a tool for in situ rock measurements usually aim for horizontal surfaces with a vertical impact without normalizing the results (E.g.: Matthews and Owen, 2010; Shakesby et al., 2011; Winkler et al., 2016; Marr et al., 2019). This is effective as long as every impact is vertical and requires a sufficient number of horizontal surfaces of high quality. It should also be clearly indicated if the results are normalized or not.

2.6 The Schmidt hammer exposure age dating technique

The first use of the Schmidt hammer for relative age dating was performed in 1984 by Matthews and Shakesby (1984). The initial idea was to chronological arrange objects and events on an ordinal timescale. The method evolved and the most recent advances in Schmidt hammer dating was introduced by Matthews and Owen (2010) and further developed by Matthews and Winkler (2011) and Matthews and McEwen (2013). The development includes the transition to a quantitative determination of the age, including uncertainties and error estimates.

The method is based on a time-dependent reduction of R-value as a surface is exposed to sub-aerial weathering (Matthews and Winkler, 2021). It revolves around establishing a linear calibration equation based on two individual sites; an older and a younger control site, whereas the younger is from a more recent event than the youngest surface to be dated and vice versa. In this way a quantitative relationship between age and R-value can be established by applying the calibration equation with the measured R-value from the surface with an unknown age. The confidence of the control sites should be as high as possible to diminish the uncertainty they may provide to the method.
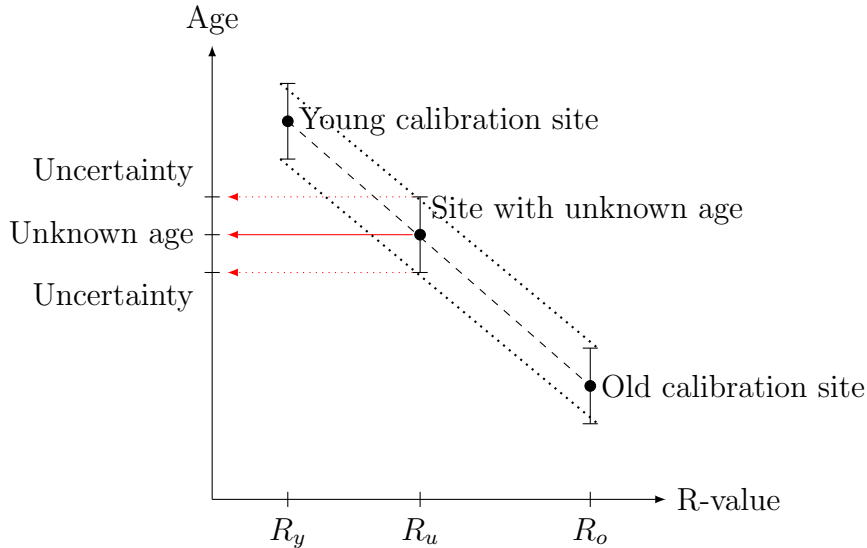
Figure 7: Illustration of the Schmidt hammer exposure age dating technique. Two sites of known age and R-value are used to find the age and uncertainties of a site with a known R-value.

To collect data for the analysis multiple blows are performed on each study site. A sample size between 25 and 150 boulders gives a stable result with indistinguishable statistical variation (Shakesby et al., 2006). The R-value for one site is the average of all measurements.

Figure 7 demonstrates how the method is applied to determine the age of a point with an unknown age.

A straight line is drawn from the youngest to the oldest control site. For the method to yield accurate ages, it has to be assumed a linear weathering rate in the range between the control sites. Matthews et al. (2020a) justifies the assumption of a linear trend between age and R-value decrease as a linear relationship is to be expected over short timescales for resistant lithologies subject to relatively slow rates of chemical weathering in periglacial environments. Furthermore empirical tests have confirmed a linear decrease of R-value with age in the Holocene timescale (Shakesby et al., 2011, Tomkins et al., 2017).

2.6.1 The use of calibration sites

The calibration sites should include two deposits of different age. The age difference should be large enough to see a significant contrast in R-value to establish a good calibration curve. The typical range of the old control sites are between 9000 and 13 000 years and the young control sites between 0 and 300 years (E.g.: Shakesby et al., 2011; Matthews and Winkler, 2011; Matthews and McEwen, 2013; Matthews et al., 2020a).

The research of Ffoulkes and Harrison (2014) is an exception to this standard, as a large number of surfaces in small age range are investigated and an old control surface of relatively young age is therefore applied.

The nature of the control sites can also influence the calibration. For young control sites, various types have been used. They can be categorized into four main groups:

1. Recent rock slope failures exposing fresh surfaces

2. Young moraines

3. Glacially scoured bedrock

4. Road cuts

The key distinction between these types lies in the surface roughness. The polished surfaces from for example glacially scoured bedrock should give higher R-values due to the removal of irregularities (Matthews et al., 2018).

For the old control sites a definite age may be more difficult to obtain as they are not on a historical record and consequently, other methods are necessary to determine their age with a larger margin of uncertainty. Examples of methods to determine old control sites is by TCN or radiocarbon dating (E.g.: Aa et al., 2007; Matthews et al., 2014; Wilson et al., 2019) and timing of glacial retreat (E.g.: Matthews and Owen, 2010; Matthews et al., 2019; Matthews et al., 2020a). The latter with a cluster of sites around 9700 years old.

2.6.2 Calibration equation

A calibration equation is used to determine the age of the investigated surface. The calibration equation represents the dashed line between the control sites in figure 7. Given the two control sites with different ages and R-values, a calibration equation can be established (Matthews and Owen, 2010). The equation is based on the linear regression equation:

$$Y = a + bX \tag{8}$$

Where Y = surface age in years, a = intersection point of the calibration curve and the y-axis, b = slope of the line and X = is the average R-value of the measured surface. The b-value is found by the two control sites and is defined by:

$$b = (y_1 - y_2)/(x_1 - x_2) \tag{9}$$

Where x_1 and y_1 represents the average R-value and age of the old control site and x_2 and y_2 the average R-value and age of the young control site.

The intersection point, a, may now be found by substitution in the calibration equation.

2.6.3 Uncertainty and confidence intervals

The method is usually given with a 95% confidence interval. A method to develop confidence intervals (C_t) with respect to the error of the calibration curve (C_c) and the sampling error of the site tobe dated (C_s) has been developed specially for the Schmidt hammer exposure age dating technique (Matthews and Owen, 2010; Matthews and Winkler, 2011; Matthews and McEwen, 2013).

As the data does not have a set population standard deviation, the confidence intervals of the two calibration sites are determined by equation (5). The error of the calibration curve is calculated according to:

$$C_c = C_o - \left(\frac{C_o - C_y}{R_y - R_o} \right) \cdot (R_s - R_o) \qquad (10)$$

where C_0 and C_y is the 95% confidence interval for the old and the young control site accordingly. R_0 and R_y are the R-values for the old and young control sites and R_s the R-value for the test site.

The uncertainty of the sample (C_s) is based on the t-distribution confidence intervals of the dating site according to equation (5) and the slope of the calibration curve (b):

$$C_s = b \left[\frac{ts}{\sqrt{n_s - 1}} \right] \qquad (11)$$

where t is the appropriate student's t-value for the degrees of freedom and confidence level, s is the sample standard deviation and n_s is the number data for the sample site. The total error is calculated by:

$$C_t = \sqrt{C_c^2 + C_s^2} \qquad (12)$$

3   Study area and geology

The study area stretches over four adjacent valleys and some surrounding areas in western Norway: Romsdalen, Eikesdalen, Sunndalen and Innerdalen (Figure 8). The area is well explored and multiple rock slope failures is detected. A large number of these are already investigated and dated. Figure 8 illustrates their placement.

The valleys in western Norway exhibit the characteristic features of alpine landscapes, featuring steep walls descending down to flat valley bottoms, sculpted by glacial activity during the last ice age.

The most recent deglaciation of the deep valleys of western Norway started towards the end of the Younger Dryas period 12 800 - 11 600 years ago, the last cold period during the last ice age (Ramberg et al., 2013; Mangerud, 2024). 12 000 years ago the glaciers covered large parts of the valleys in the study area. The melting process diminished the glacial extent, and by 10 700 years ago the study area were nearly free for glaciers (Hughes et al., 2015; Romundset et al., 2023) .

The glacial extension and retreat is a recurring cycle where glaciers carve steep valleys in the landscape. This leads to destabilization of rock slopes after deglaciation due to loss of permafrost and support from the glaciers in the valley Kos et al., 2016. The valleys of western Norway is a good example of this process and therefore provide an ideal setting for the study of landslides. With each new glaciation, evidence of past landslides is erased through glacial erosion and transport. Consequently, the majority of landslides observed in these valleys date back to the Holocene, after the last glacial retreat.
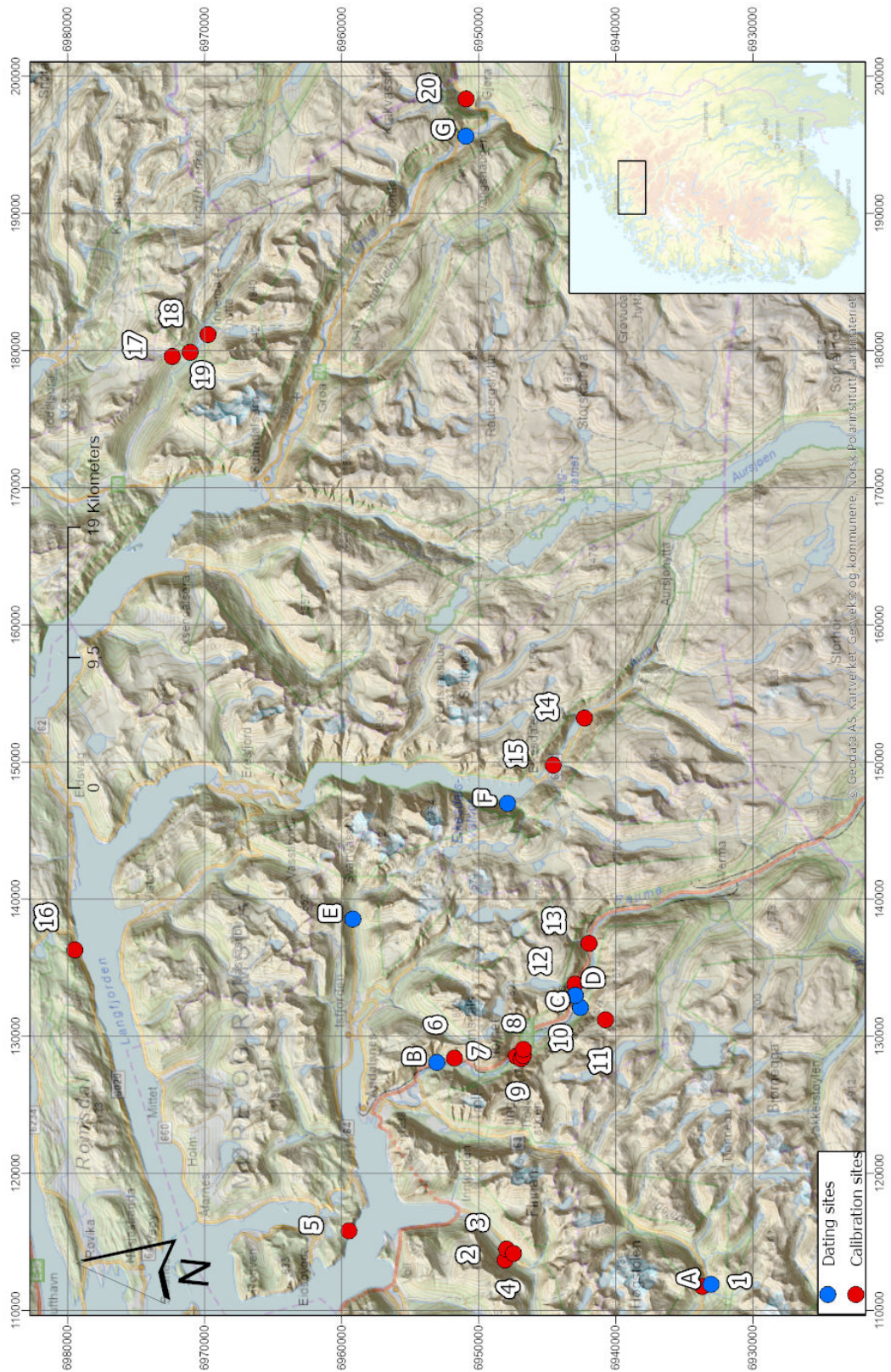
Figure 8: Map with calibration sites and dating sites included in this study. Calibration sites are deposits already dated in other studies, while dating sites are deposits without a known age.

The study area lies within the county of Møre og Romsdal, which is part of the western gneiss region of Norway. The region consists of different kinds of gneiss and migmatic rocks of proterozoic age which underwent metamorphism and deformation during the Caledonian mountain-building event around 490 – 390 million years ago (Ramberg et al., 2013). The bedrock map from NGU (Figure 9) shows how the test sites mainly consist of three different sub-lithologies of gneiss:

1) Granitic ortogneiss and migmatic gneiss.

2) Granitic gneiss and coarse grained granite.

3) Silimanitic gneiss.

Figure 9 gives an overview over test sites and the local lithology recorded by NGU.
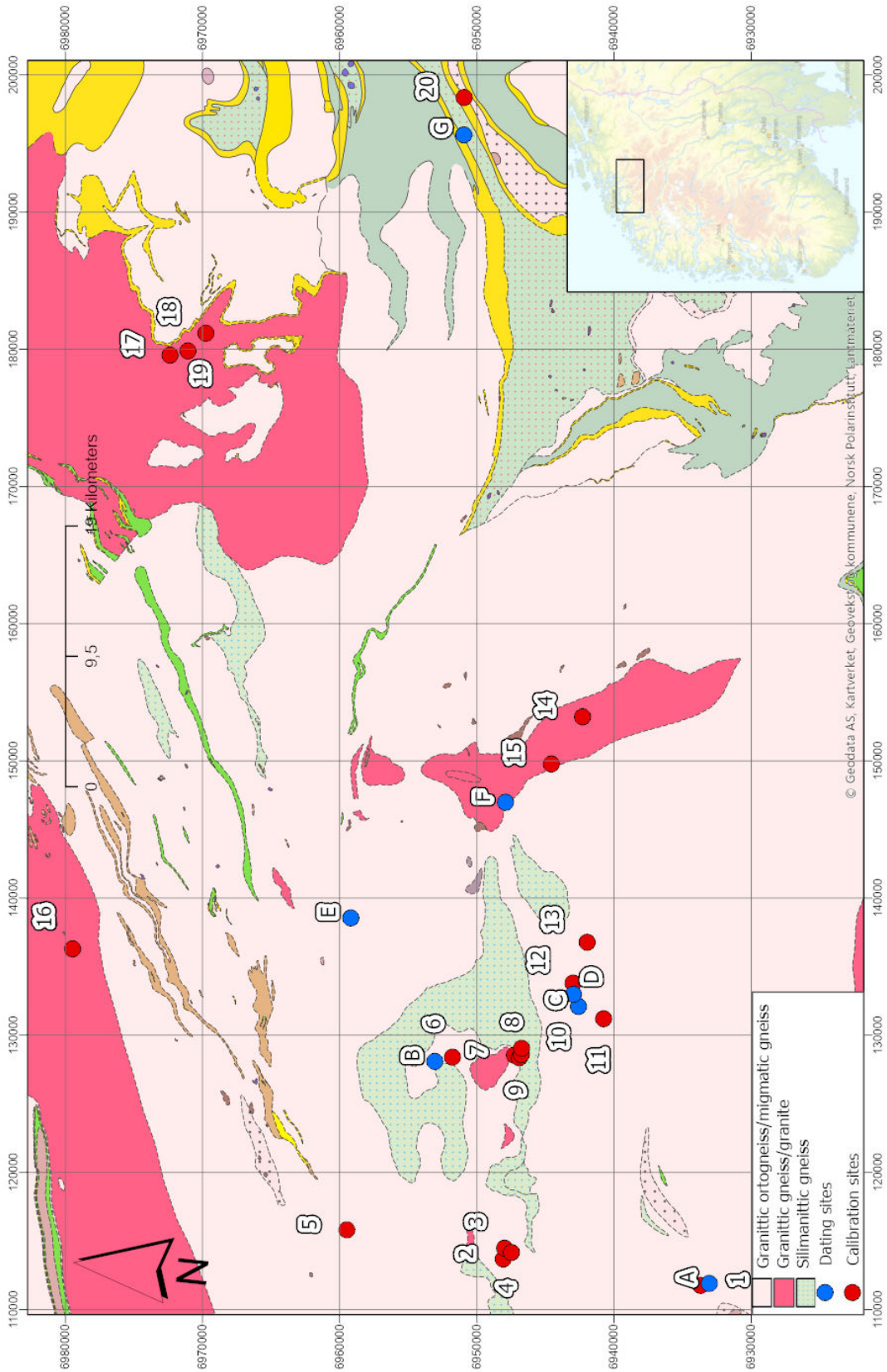
Figure 9: Map with the local lithology as described by NGU.

3.1 Calibration sites

The different test sites as shown in figure 8 are locations already described in previous literature. This chapter will offer a brief description of the most important characteristics of each site. All deposits dated by using ^{10}Be dating, were calculated anew in this thesis using the online calculator which can be found in Balco et al. (2007) and are given here with LSDn scaling scheme (Balco et al., 2007). The ages are therefore slightly different from the ages found in each publication. The presented dates in this chapter are the ages described in the publications, while table 3 lists the recalculated ages. A table containing coordinates and dating technique applied for each site is available in appendix A.

3.1.1 Alstadfjellet

Alstadfjellet is a large rock avalanche deposit located between 300 and 600 meters above sea level close to Valldal. The deposit may be seen while travelling along the road between Trollstigen and Valldal. A wedge shaped failure scar (Figure 10) is visible with a 1.5 km^3 debris lobe consisting of large boulder. The deposit extends over and continues up on the opposite side of the valley. The site was first dated by Hermanns et al. (2017) and is described by Wilson et al. (2019), where a comparative surface dating of the SHD technique and ^{10}Be dating was performed. The obtained results gave a SHD age of 10.3 ± 0.59 - 11.1 ± 0.64 ka and ^{10}Be age of 9.2 ± 0.7 - 9.8 ± 0.7 ka.
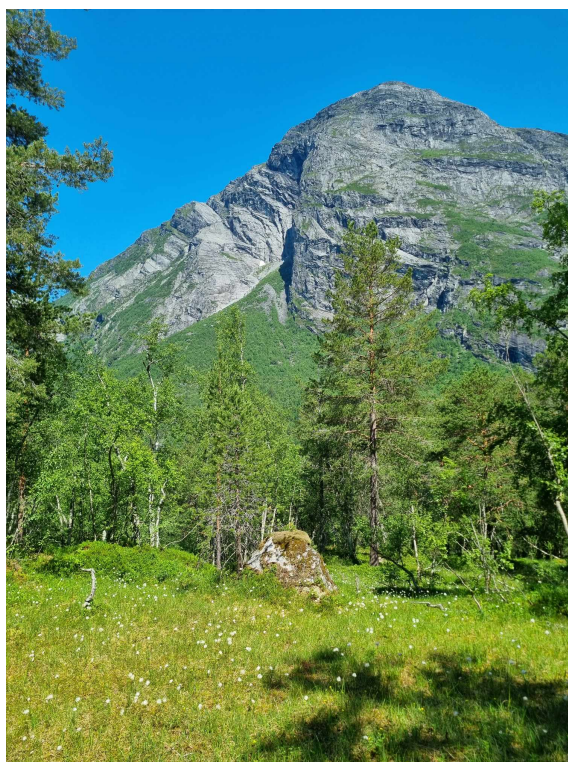
Figure 10: Alstadfjellet. A wedge shaped failure scar is visible in the mountain side. Picture take from the east side of the mountain looking west.

Granitic ortogneiss/
migmatic gneiss

Number	Site	Age (years)	Uncertainty (±)	Reference
1	Alstadfjellet	9000	700	Wilson et al., 2019
2	Gråfonnfjellet old	13750	1200	Schleier et al., 2017
3	Gråfonnfjellet middle	7650	650	Schleier et al., 2017
4	Gråfonnfjellet young	500	100	Schleier et al., 2017
5	Gråura	14050	1750	Hermanns et al., 2017
6	Venja	1600	400	Blikra et al., 2006
11	Svarttinden	9500	750	Hermanns et al., 2017
12	Mongefossen	3	0	Historical event
13	Skiri	11100	600	Hermanns et al., 2017
20	Ivasnasen	3300	350	Oppikofer et al., 2017

Granitic gneiss/granite

Number	Site	Age (years)	Uncertainty (±)	Reference
14	Setra, Eikesdalen	12600	1000	Pers. communication
15	Hølsteingjerdet, Eikesdalen	2000	250	Pers. communication
16	Tjellefonna	270	0	Historical event
17	Isolated boulder patch, Innerdalen	13500	1000	Schleier et al., 2015
18	Innerdalsvatnet	7950	950	Schleier et al., 2015
19	Fluotjønna, Innerdalen	7550	600	Schleier et al., 2015

Silimanitic gneiss

Number	Site	Age (years)	Uncertainty (±)	Reference
7	Mann23	5300	400	Hilger et al., 2018
8	Mann31	5200	400	Hilger et al., 2018
9	Mann36	9450	700	Hilger et al., 2018
10	Mann38	5150	400	Hilger et al., 2018

Table 3: All dated deposits investigated including reference to their respective publication. The three seperate tables represents the three lithological domains the different sites belong to. ^{10}Be ages are calibrated by the LSDn scaling scheme according to Balco et al. (2007) using the online calculator.

3.1.2 Gråfonnfjellet

Gråfonnfjellet is located in Innfjord-
dalen close to Åndalsnes in Romsdalen. Innfjorddalen Valley is characterized by its
glacially sculpted U-shaped cross-profile and a significant topographic relief. The
mountain itself stands at 1475 m.a.s.l on the southern side of the valley. A promin-
ent scar is clearly visible in the mountain with large rock avalanche deposits covering
the valley beneath.

Schleier et al. (2017) has worked at dating multiple deposits to determine the evolu-
tion of the valley and temporal occurrence of the different rock avalanches. Multiple
TCN tests were performed on a number of sites in the different deposits. Three
main events were identified:

1. The first event happened 14.3 ± 1.4 ka. A unique aspect of this event is that
   it entered while the valley was still a fjord, subsequently raised above sea level
   due to post glacial isostatic rebound. While entering the shallow fjord some of
   the material went through the water masses to finally deposit on the opposite
   facing slope of the valley. This is evident by a clear ridge shaped structure.
   The parts of the deposit beneath the pre-isostatic rebound water level shows
   a lower age, as Schleier et al. (2017) argues may come from the shorter time
   of exposure to cosmogenic nuclides. This may also affect the weathering rate
   and thus the Schmidt hammer rebound value. To make sure to obtain a higher
   probability of a correct age Schmidt hammer blows was performed on the parts
   of the deposit reaching over the former water level at the opposite side of the
   valley.

2. The second deposit overlays the first one and dammed a lake that still exists
   to a certain degree at the present. This deposit is dated to 8.79 ± 0.94 ka
   (Schleier et al., 2017).

3. This is the stratigraphically highest deposit and also the youngest dated to
   500 ± 100 years. Compared to the two first deposits it is a lack of forest cover
   which corresponds well with the younger age. This deposit is also expected

to be related to a historical event from around 1611 (Furseth, 2006) and the TCN-age confirms this possibility.

3.1.3 Gråura

This deposit can be found on a 440 m high peninsula between Langfjorden and Romsdalsfjorden. It has a H/L ratio of 0.45 and a lobate form without any talus cone, and can therefore be categorized as a rock avalanche (Hermanns et al., 2017). [10]Be ages from samples of the frontal part give a deposit mean age of 14.1 ± 1.9 ka years.

3.1.4 Venja

The Venja deposit is situated in the northern side of Romsdalen, close to Åndalsnes. Blikra et al. (2006) describes Venja as a typical landslide into a sediment filled valley bottom. Furthermore, from sea level analysis they suggest the deposit is younger than 2000 years and which is confirmed by ^{14}C-dating of charcoal found below the deposit giving estimated ages of 1992-1882 and 1413-1352 years. An approximate age of 1600 ± 400 is there for a reasonable estimate for the age of event.

3.1.5 The Mannen-Børa complex

The Mannen-Børa complex is a large unstable rock slope on the southern side of Romsdalen (NVE, n.d.). A movement of 2 cm/year is registered and an absolute failure would have large consequences for the inhabitants of the valley beneath and the village of Åndalsnes.

Multiple rock slope failure deposits are mapped along the valley floor below the unstable slope, indicating prior instabilities and failures (Hilger et al., 2018). The deposits are recognized and dated by Hilger et al. (2018). Four of these sites were included as Schmidt hammer test sites in this study (table 3).

3.1.6 Skiri

The Skiri rock avalanche is a large deposit of boulders extending over a large part of Romsdalen. The deposit is interpreted as remains from two seperate large events byHermanns et al. (2017) with ages of 11.0 ± 1.3 ka years for the western part and 11.7 ± 1.3 ka years for the eastern part of the deposit. For this study only the eastern part of the deposit was investigated.

3.1.7 Mongefossen
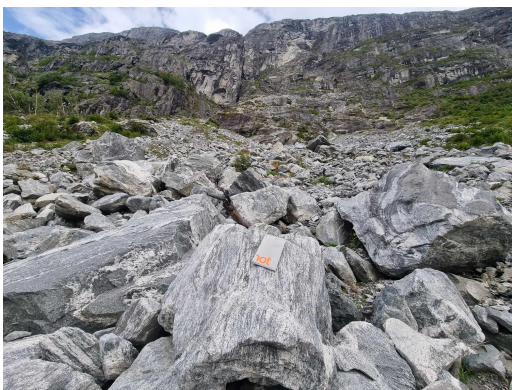
(a)
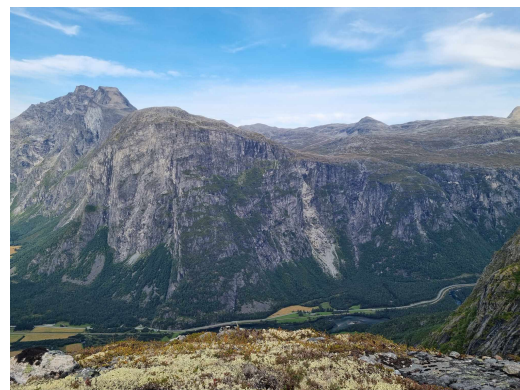
(b)

Figure 11: a: Looking up on the fresh rock slide by Mongefossen. b: The rock slide seen from the southern side of the valley looking north.

On the 23rd of October 2020 a rock slide occurred near Mongefossen in Romsdalen (Ørjaseter, 2020). The site is visible from the other side of the valley and is a located only a short hike from the main road through Romsdalen.

3.1.8 Svarttinden

The Svarttinden deposit is found on a large plateau at 1100 m.a.s.l, directly above the southern side of Romsdalen. A large failure scar is apparent in the peak of Svarttinden with a large deposit covering the plateau underneath. The outermost part of the deposit reaches the edge of the plateau. The deposit is clearly visible as there is no vegetation cover at this altitude (Figure 12). [10]Be ages recorded by Hermanns et al. (2017) gives an average age of 8.7 ± 1.1 ka years.

Figure 12: The deposit of the rock avalanche seen from the top of Svarttinden. The deposit extends over the plateau before dipping slightly over the edge down to Romsdalen.

3.1.9 Eikesdalen

Eikesdalen is a steep valley with multiple rock avalanche deposits visible throughout the area. In one area, several larger deposits cover the valley floor, including parts of the Digerura deposit. Tree trunks fond underneath the sub-aqueous part of this deposits were dated by Austigard (2016), estimating the deposit's age to be around 2500 years. Unpublished [10]Be ages has been conveyed by personal communication by Reginald Hermanns from a recent investigation of the multiple rock avalanche deposits. Hølsteingjerdet, a site near Digerura, has a TCN-age of 2000 ± 250 years, while another nearby site, Setra, has a TCN-age of 12600 ± 1000 years. This data indicates that multiple large events have occurred throughout the late Younger Dryas and the Holocene.

3.1.10 Tjellefonna

On 22 of February 1756 a large rock avalanche occured on the northern side of Langfjorden close to Tjelle. Volume estimates of the event ranges between 9.3 to 10.4 million m^3 and the large rock masses created three large displacement waves which lead to massive destruction and the loss of 32 human lives (Sandøy et al., 2016).

3.1.11 Innerdalen

Innerdalen is located near Sunndalsøra and is an east-west reaching valley. Multiple signs of former glaciation and rock slope failure events is visible in the valley. Large moraines with rock boulders and rock slope failures deposited far up on the opposite side of the valley also indicates failures happening before and during glaciation (Schleier et al., 2015).

Three different deposits were examined by Schmidt hammer dating: Two of the deposits are located near Innerdalsvatnet and one deposit is found on the south facing slope. The latter is depicted as an isolated boulder patch deposited from an event during the glaciation (Schleier et al., 2015) This boulder patch also excels due to mainly consisting of quartzitic boulders.

Schleier et al. (2015) has performed TCN-dating in the area to determine the ages of the different deposits. Ages can be found in table 3.

3.1.12 Ivasnasen

Ivasnasen is located close to Gjøra in Sunndalen. A rock avalance deposit can be seen on the southern side of the valley, and is easily accesible from the main road from Oppdal to Sunndalsøra. On the bedrock map of NGU (Figure 9) it is located within different lithologies, but as described by Oppikofer et al. (2017), the deposit is mainly composited of augen gneiss. Oppikofer et al. (2017) has dated the deposit by [10]Be dating giving an estimated age of 3.3 ± 0.1 ka years since failure.

3.2 Undated deposits

Measurement of the R-value of 7 undated deposits in the study area were performed. All deposits is categorised as rock avalanches and their location can be found in figure 9. Table 4 presents the undated deposits and their lithology.

Letter	Site	Lithology
A	Alstadfjellet undated	Granitic gneiss/migmatic ortogneiss
B	Tomberg	Granitic gneiss/migmatic ortogneiss
C	Remmem	Granitic gneiss/migmatic ortogneiss
D	Mona	Granitic gneiss/migmatic ortogneiss
E	Isfjorden	Granitic gneiss/migmatic ortogneiss
F	Mardalen	Granitic gneiss/granite
G	Gravemsura	Silimanitic gneiss/augengneiss

Table 4: Overview of the undated deposits investigated in the study area

Alstadfjellet undated is a deposit from same source as the dated Alstadfjellet deposit. This deposit reaches further up on the opposite valley side, indicating an event occurring prior to the event described in chapter 3.1.1

4   Method

4.1   Location of calibration sites

Large rock slope failures can be distinguished both in the field and on a digital terrain model. For the study area this work is already performed by Penna et al. (2022) which makes the process of finding the localities easy. Figure 13 demonstrates where the different deposits were found according to Penna et al. (2022).

4.2   Field work

The Schmidt hammer measurements performed during the field work were based on the description on how to use a Schmidt hammer to measure R-values by Aydin and Basu (2005). Mechanical N-type Schmidt hammers from the manufacturer Proceq were used, as compared to the L-type hammers gives a higher impact energy and is therefore better suited for hard rock types as gneiss (Aydin and Basu, 2005).

It is recommended to have a large sample size to account for the variability within a site (Matthews and Winkler, 2021). It was chosen to investigate 50 boulders for each site. 2 blows were performed on each boulder, giving a total of 100 R-values at each site.

The blows were performed only on boulders larger than 1m^3 to avoid the loss of energy by movement of the boulder. The test sites used also excluded edges, cracks, joints, irregularities, large mineral grains, and unstable boulders (Shakesby et al., 2006; Matthews and Owen, 2010; Marr et al., 2019). Moisture was avoided, as it is expected to influence the R-value (Aydin and Basu, 2005). Efforts were made to avoid lichen presence. However, at certain sites, lichen abundance posed challenges. Consequently, a few R-values may have been measured on surfaces with limited lichen coverage.

Only vertical impacts on horizontal surfaces were performed to avoid further complexity to the method and reducing the amount of potential sources of error.
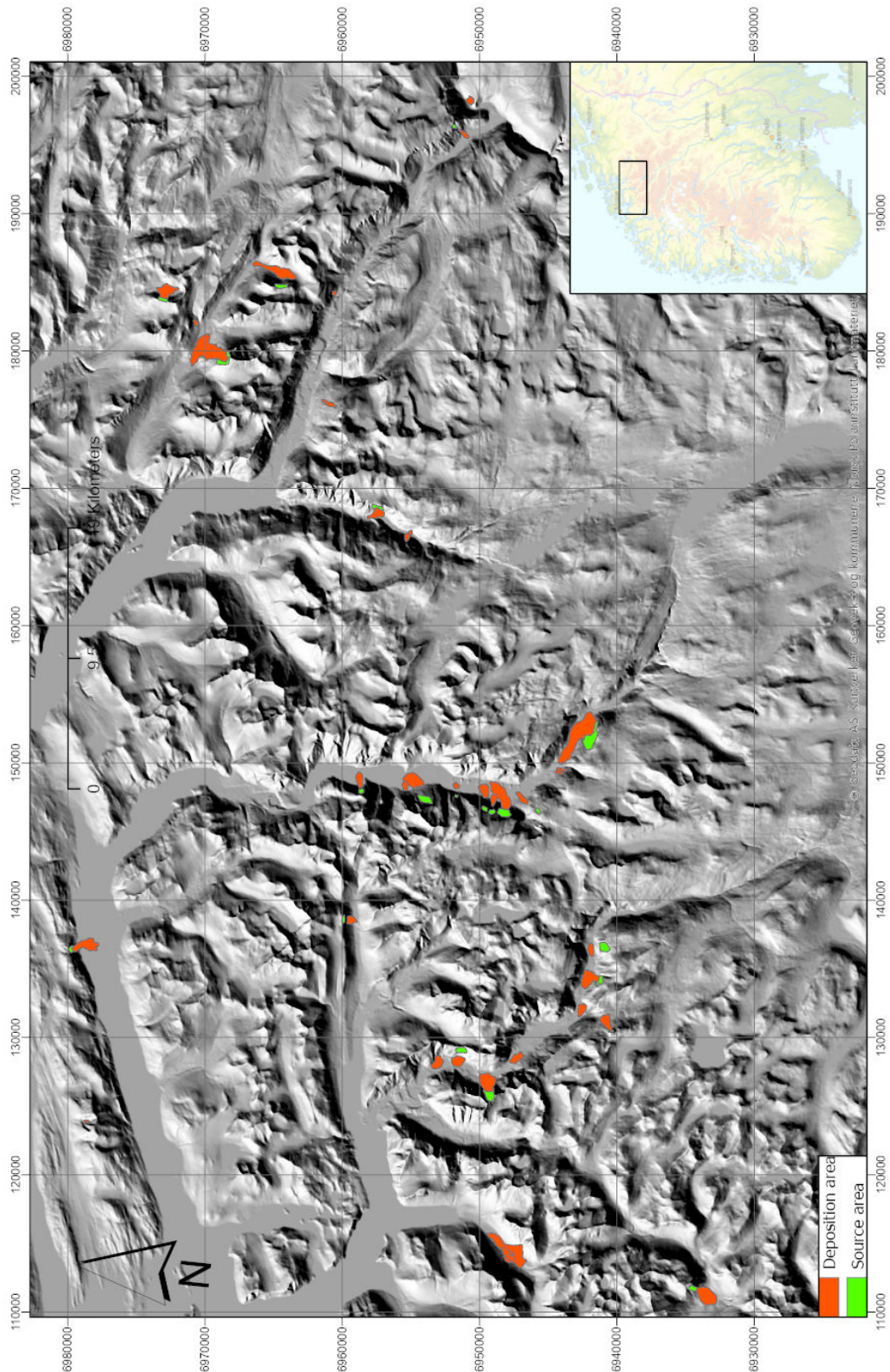
Figure 13: Location of the rock slope failures in Romsdalen, Eikesdalen, Sunndalen, Innerdalen and surrounding areas as mapped by Penna et al. (2022)

For the method to achieve universal applicability, it is essential to maintain absolute objectivity. Therefore, any R-value readings that may appear erroneous due to unknown reasons were included in the results. Exceptions were made only when clear indicators of methodological interference, such as audible echoes from underlying joints or cracks, were present (Matthews and Owen, 2010).

At the location of Gråfonnfjellet old a sample of a tree was taken for radiocarbon-dating. This analysis was performed by the NTNU lab for radiocarbon dating (Lab number of sample: TRa-226993).

Some alternative methods were also tested. For some calibration sites the L-hammer was used in addition to the N-hammer and plotted as separate results. The purpose was to test if the L-hammer could give valid results for these lithologies. The methodology were the same as for the N-hammer. The included sites were Alstadfjellet, Skiri, Mongefossen and Gråura.

Aydin and Basu (2005) suggest that an effective method to determine the degree of weathering may be to hit the same spot twice. The first hit will remove the outermost weathered layer and the second will then give a higher R-value. The difference in the values between the first and second impact may give an indication of the weathering condition of the surface. Matthews and Winkler (2021) also shows how a second impact on the same spot gives an increased R-value. This method was further investigated to evaluate if it could provide a better correlation for the determination of the age. For multiple sites each surface were therefore impacted twice on the exact same spot. In contrast to the traditional Schmidt hammer dating method by one impact on each surface, an increase of the value by higher age is to be expected. This is a result of a longer time of weathering and should result in a higher difference between the first and second impact.

4.3 Sources of error during the field work

Several factors can introduce uncertainties into the testing process, affecting the reliability and accuracy of the results. These uncertainties primarily stem from variations in different properties of the tested material as the hammer is a sensitive

instruments where even minor variations may affect the rebound value significantly. At the same time the hammer itself may be worn after some usage and contribute with uncertainties.

Roughness of the rock surface can significantly influence Schmidt Hammer test results. Irregularities on the surface can cause the hammer to rebound unevenly, leading to variations in measured values. High surface roughness may result in increased scatter in the data and reduced repeatability of measurements. It has been suggested that the error limits could be further improved by using smooth, glacially polished bedrock surfaces, particularly as control sites as the amount of irregularities are smaller than unpolished surfaces (Owen et al., 2007; Matthews and Owen, 2010; Matthews and Winkler, 2021).

Lithological variation may appear within a study site. Gneiss is a heterogeneous metamorphic rock, containing bands and layers of different mineral compositions and textures (Raade and Fossen, 2020). As independent minerals gives a different rebound due to their difference in hardness, this can lead to inconsistency in the measured R-value throughout a study site.

Boulder size can affect the value as if the boulder is too small some of the energy can be lost instead of rebounded from the hammer (Aydin and Basu, 2005).

Altitude and climate may have an effect on the weathering rate. Existing studies suggests that local climatic variability has little effect on the R-value and is insifnificant compared to the geological variability (Matthews and Winkler, 2021). Zasadni and Kłapyta (2016) found how altitude and R-value had a very poor correlation, and therefore the R-value is mainly affected by the time of exposure.

Deviations in the instrument can occur over time. As the hammer performs a large number of blows the spring may become worn and therefore give different R-values. Water, particles and dust may enter the housing to cause larger friction and lower the R-values. To monitor the hammer deviations 20 blows on the manufacturers test anvil was performed between each study site (Matthews et al., 2015; Matthews and Winkler, 2021). The hammer should stay within limit of 81 ± 2 (Proceq, 2002). A drift was seen over time in the hammer, where the anvil test gave lower values

after some use. The drift was corrected relative to the deviation from the expected value of the anvil test. This was performed according to the formula:

$$R_n * (R_A/81) \tag{13}$$

Where R_n is each R value and R_A is the average anvil value after 20 impacts. Values below 79 were also accepted as long as the hammer gave reliable values on the anvil test (± 2). This acceptance of of lower values with good consistency will be further discussed. At occasions the calibration test deviated more than acceptable and the test sites performed after this were regarded as invalid and not used for further analysis. A new hammer was bought the first time the deviation was too large, whereas the second time the hammer was sent to the manufacturer for re-calibration.

The Schmidt hammer tests were conducted by four different individuals during the fieldwork, potentially introducing variability in the measured values due to differences in operating techniques. All operators received identical training and had the same level of knowledge regarding the testing procedures. The measurements were performed under the supervision of other team members, who recorded the instrument readings. Additionally anvil tests were performed by all operators and the readings were similar. It is crucial for the reliability of the method that individual differences do not significantly influence the results, as this could compromise the objectivity of the method and limit the applicability of calibration equations to specific operators. As this study seeks to determine the universal applicability of the method it was assumed that similar training and knowledge is enough to neglect individual operator differences.

4.4 Research design

The study area contains multiple already dated and historical recorded deposits of ages ranging from 3 to 14,000 years old. It was aimed for an approach which distinguishes itself from prior studies by applying a spectrum of ages rather than

merely featuring one old and one young control surface. By incorporating this wide range of ages, it opens up the opportunity to thoroughly analyze the method's effectiveness and analyze the validity of the assumption of a linear trend.

Matthews et al. (2020a) use smooth and polished surfaces as this includes less irregularities, while Matthews et al. (2018) prioritise young control sites of similar properties as the rock slope failures they want to date, as this would have the same prerequisites. The use of deposits made by the same processes for all study sites is the best approach to have the relative same amount of irregularities affecting the results (Matthews and McEwen, 2013; Matthews and Winkler, 2021). Therefore, the control sites chosen for this analysis exclusively involves rock slope failure deposits, to give priority to a selection which ensures that the control points exhibit comparable characteristics in terms of nature and roughness as the surfaces to be dated. Consequently, the calibration equations and techniques developed in this study may not be applicable for dating other types of landforms and deposits within the same region or lithology.

The different dating sites and their characteristics are described in section 3.1. The ages are known through historical records for younger rock slope failures and radiocarbon dating and TCN dating for older deposits.

In the method developed by Matthews and Owen (2010) the age is on the y-axis and the R-value on the x-axis of the graph and also used this way in the calibration equation. In this study it is chosen to change the axes to obtain a more intuitive representation of age along the horizontal axis for the visual presentation of the data. The calculations are still performed as if the age is on the y-axis and therefore no change in the calibration equation is necessary. Changing the axes for the calculations would make the slope of the calibration line much smaller, thus equation (11) becomes implausible.

As the population standard deviation is unknown, the sample s was found for the test sites. As a result the confidence intervals for the mean of the dating sites were calculated by applying the Student's t-distribution according to equation (5). The number of data (n) for each test site is 100, giving 99 degrees of freedom. The

corresponding t-value was found for the degrees of freedom and the wanted level of confidence.

4.4.1 Analysis of the data

Scatter plots were constructed for all the data. Separate scatter plots for different lithological units were also constructed to analyse the impact of different lithology between the study sites. Additionally scatter plots for the L-hammer and the double-hit method were made.

Illustrations of the results were made using Python code. Calibration of the R-values was performed in Microsoft Excel. The calibrated R-values were read from an Excel-sheet using the Pandas-module in Python. Necessary calculations of means, medians and mathematical operations for the uncertainties were performed by the Numpy-module and graphical outputs were constructed using matplotlib.pyplot.

To assure that the output of the Python codes were accurate, some of the graphs were also constructed in Microsoft Excel as a quality control.

Histograms showing the distribution of the data from each site were constructed and exported directly from Microsoft Excel.

One way to test the accuracy of the method is to select an old and a young calibration site from the data and control if they would be able to correctly estimate the age of a third deposit by applying the method of Matthews and Owen, 2010. To do this once would require a subjective selection of three deposits; old, young and deposit to date. The choice of these deposits would highly influence the outcome of the test. To avoid the problem of having to choose deposits, a Python script was made to iterate through every deposit using every possible combination of young calibration site, old calibration site and deposit between them. If the calculated age (Equation 8) $\pm$ the uncertainty limit C_t (Equation 12) overlaps the age $\pm$ uncertainty described by from table 3, the code returns the estimated value as correct. If they do not overlap, it returns the value as incorrect. The number of correct and incorrect values were counted to determine how many of the deposits the method were able to estimate

an assumed correct age for.

As described in chapter 2.6.1, the typical age range of the old control sites is between 9000 and 13 000 years and the young control sites between 0 and 300 years (E.g.: Shakesby et al., 2011; Matthews and Winkler, 2011; Matthews and McEwen, 2013; Matthews et al., 2020a). Therefore ages below 400 years were chosen as young control sites, while ages above 9000 years were chosen as old control sites. Ages between 300 and 9000 years were treated as deposits with an unknown age where the age was calculated and compared with the age from table 3.

Maps and analysis of deglaciation were performed in ArcGIS pro. Data from the Dated-1 database (Hughes et al., 2015) were imported and compared directly to the estimated ages of the rock slope failures in the study area.

4.4.2 Statistical tests

Two different statistical tests were performed on the data. The correlation coefficient and the corresponding p-value was found using the Kendall's τ correlation test (Penna et al., 2023). This test was chosen as it is independent of data type and variability, and is therefore more robust when dealing with data of an unknown distribution (Penna et al., 2023). The Shapiro-Wilks test was applied to determine how close the data were to a normal distribution, and hence if the mean and its confidence interval could be used with certainty. The confidence intervals were calculated using the Student's t-distribution (Equation 5), but as the number of Schmidt hammer blows n > 30 it could be assumed that the t-distribution and normal distribution were nearly equal (Løvås, 2018). Both of the tests were performed by a Python code using the scipy.stats-module.

5 Results

5.1 Discarded values

Precautions should always be taken before discarding values. Discarding outliers without good reasoning could hurt the integrity of the work. After careful consideration, two sites were discarded from the results: The oldest deposit by Gråfonnfjellet and the isolated boulder patch in Innderdalen (Table 3).

5.1.1 Isolated boulder patch, Innerdalen

During sampling of the isolated boulder patch, suspiciously high R-values were measured compared to the ^{10}Be surface exposure age of 14100 ± 400 years. Data treatment gave an average R-value of 51.3. Such values were normally found on deposits with an age of 0 to 300 years.

A lot of quartz were detected during sampling. The bedrock map of NGU (Figure 9) shows how the deposit is in an area consisting of granitic gneiss and granite. However, Schleier et al. (2015) suggests the boulder patch mainly consists of quartzitic boulders, which corresponds with the field observations.

As quartzite is a particularly hard and compact metamorhic rock type (Haldar, 2020), higher R-values are to be expected. The high R-value from the sampling site further strengthens the assumption that harder rocks give higher R-values, but can not be compared to the R-values of the other dating sites composed of typical gneisic composition and the deposit was therefore discarded.

5.1.2 Gråfonnfjellet old

The test site of Gråfonnfjellet old is described in section 3.1.2 as a distinct ridge with large boulders on the opposite side of the valley from the failure scar. The deposit is dated to 13750 ± 1200 years (Figure 3; Schleier et al., 2017). During the field work the R-values were notably higher than expected compared to this age.

This was confirmed after data treatment which gave an average corrected R-value of 45.11.

On the site a tree trunk was found below one of the boulders. This tree trunk was deformed by the boulder impact. (Figure 14a). This further implies that the tree had a growth period before the presence of the overlying boulder. A radiocarbon age determination was performed on a sample of the tree. The results are presented in Appendix C.

(a)   (b)

Figure 14: (a) The tree stuck underneath the rock. The roots of the tree grows under the mass of the rock and can not be moved. (b) The rock where the tree can be found underneath

The radiocarbon dating suggests that the tree experienced a growth period around 1500 A.D. or 1600 A.D. Consequently, it casts doubt on the boulder's deposit age, estimated at 14.3 ± 1.4 (ka). Since there are no apparent signs of a significant event from Gråfonnfjellet during this period, an investigation of the east-facing slope became of interest as a rock boulder could have sourced from that site. Figure 15a presents the results of a rock fall simulation performed according to Noël et al. (2023) in the Innfjorddalen valley.

(a)   (b)
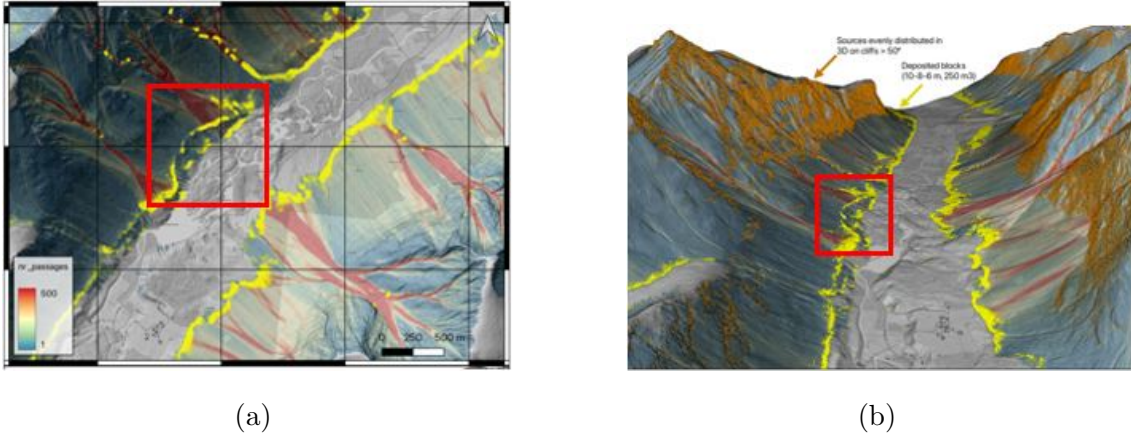
Figure 15: (a) Simulation of rock falls in Innfjorddalen. The simulation was performed by François Noël according to Noël et al. (2023). Yellow dots represent the simulated rocks. Red square marks the location of the ridge (b) The valley represented in 3D. Orange dots represent potential rockfall source areas

The simulation indicates the possibility for the ridge to work as a fence to accumulate rock falls. Based on the combination of the dated tree underneath the rock and the simulation proving the physical possibility of rocks deposited at a later time, the likelihood of a erroneous R-value is high. Thus, the site was discarded.

5.2   Calibration sites

The calibration sites are represented by the sites with an already known age as presented in Table 3. The results are presented in figure 16.
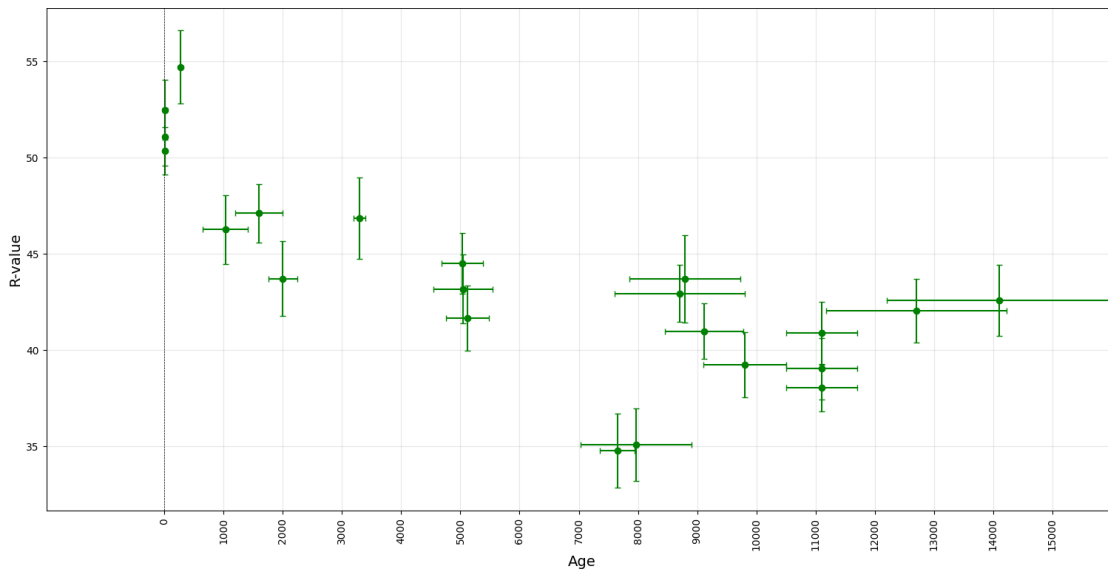

Figure 16: Calibrated R-values compared to age with uncertainties represented in table 3. Vertical uncertainties are the calculated 95% confidence interval for the 100 blows of each site.

The R value has a range between 55 and 35, with the youngest ages also giving the highest R values. As the trend is a decreasing R-value by increasing age, some clear outliers are apparent. The lowest R-values occur around an age of 8000 years. Both of these deposits are in the same area in Innerdalen and are quite significantly lower than expected for their age. There is no argument to not include these values and they will therefore stand as two outliers in the data. The two oldest deposits between 12000 to 14000 seems to have a slight increase compared to the deposits between 10000 and 12000.

A linear trend is visible in the data, but with a large spread. To understand the uncertainties of the dating sites, the individual data for each site can be analyzed. The use of the mean with confidence intervals requires a normal distributed set of data to be valid. A visual check for normality can be performed by plotting the data in histograms. Figure 17a and 17b represents the histograms from two different calibration sites.
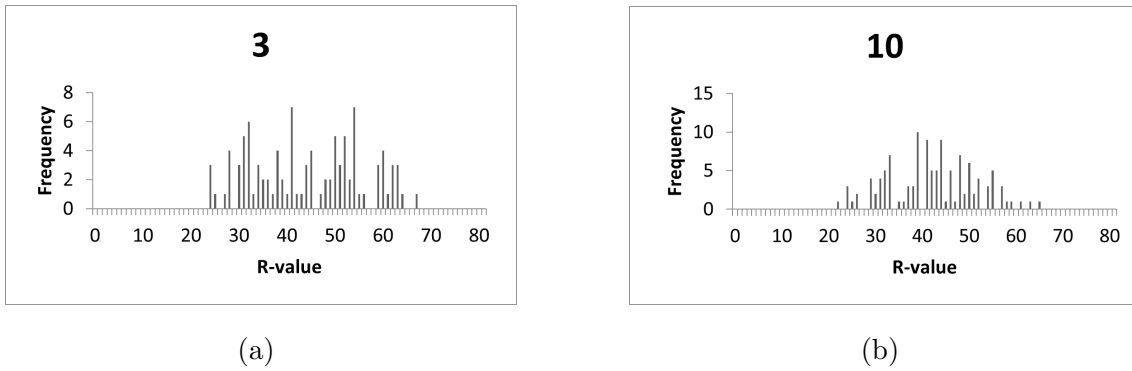
(a)	(b)

Figure 17: a: Histogram for site 3, Gråfonnfjellet middle. The shape of the data does not look like a typical normal distribution. b: Histogram for site 10, Mann 38. The shape of the data could be associated with a normal distribution form.

For the figure, two sites were chosen to represent the differences in the data. Figure 17a does not seem to show a normal distribution, with multiple peaks ranging from an R-value around 30 to 55. Figure 17b has a form more similar to a normal distribution with a higher peak between 40 and 45 with decreasing values on each side. This is also confirmed by a Shapiro-Wilk test. The test gives a P-value of 0.0016 for site 3 and a value of 0.67 for site 10. This indicates that for site 3 the null-hypothesis of a normal distribution can be rejected, while a normal distribution is possible for site 10. Appendix B presents histograms for each calibration site. The Shapiro-Wilk test p-value for each site is presented in figure 18.
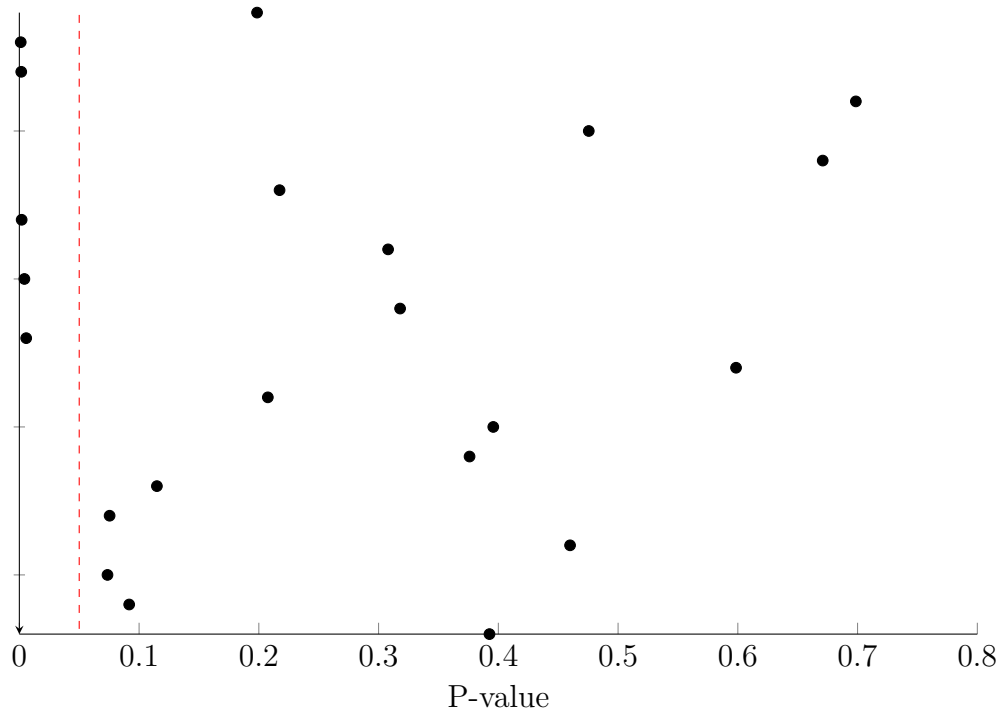
Figure 18: P-values from the Shapiro-Wilks test for each site. A low p-value indicates a higher probability of a rejection of the null-hypothesis of a normal distribution. There is 95% confidence of a rejection of the null-hypothesis for values beneath 0.05.

For a large part of the data the null-hypothesis of a normal distribution can not be rejected. Five sites are clearly not normal distributed, while four are close to the limit of 0.05. As non-normal distributed data can not be presented by mean and confidence intervals (Løvås, 2018), the data is also illustrated by a box plot with medians with percentiles. Figure 19 presents this data.
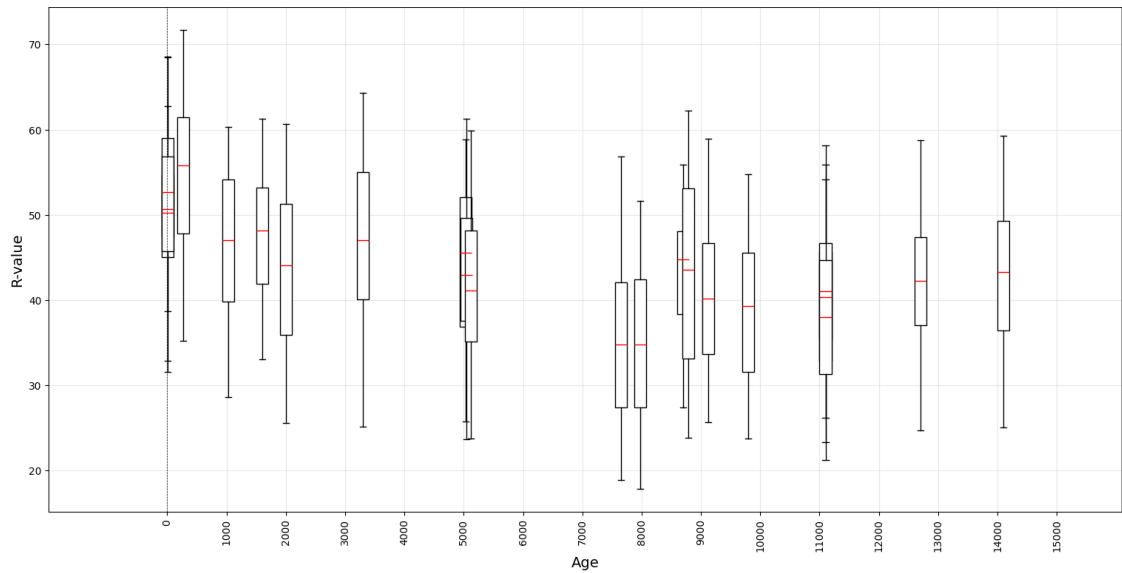
Figure 19: Plot of medians of all sites. The box edges are the 25 and 75 percentile while the whiskers extends to the 2 and 98 percentiles. Age uncertainties in x-direction are the same as for the median plot, but are removed for readability.

The plot of the median values is very similar to the plot of the mean values (Figure 16). R-values have a range between around 56 to 35. The uncertainties are larger, as should be expected when using percentiles instead of the mean with 95% confidence intervals as it cuts the data in the exact position where the chosen percentage of data falls within rather than estimating the probability of the mean to truly be in within the range (Løvås, 2018). The comparison of the median and mean with their uncertainties can be illustrated by plotting both in the same plot. This is executed in figure 20

The median is slightly different than the mean. The trend is that the median has a higher R-value, which indicates that more of the extreme values occur on the lower end of the measurements.
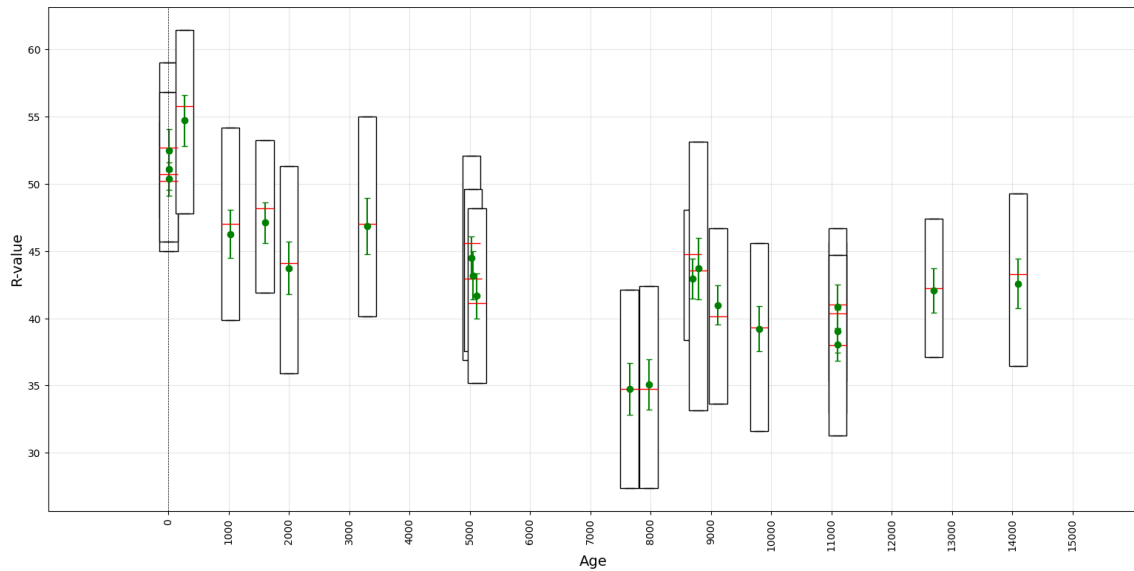
Figure 20: Plot of means and medians for all sites. Means are represented by green points with 95% confidence intervals based on the standard error of the samples, while medians are represented by red lines with boxes representing the 25th and 75th percentiles. Horizontal uncertainties for ages and whiskers for medians are removed for readability.

5.3   Lithology

Difference in lithology can significantly influence the R-value (Eg.: Aydin and Basu, 2005; Matthews and Owen, 2010; Matthews and Winkler, 2021). In order to reduce the importance of lithologic difference, the study area has been subdivided into smaller lithological units following map units chosen by NGU (Table 3). The sites with a similar lithology are aggregated within the same plots in figure 21 (mean) and figure 22 (median).

The plots reveal that there are more sites in regions consisting of granitic ortogneiss and migmatic gneiss compared to the two other geological domains. More data enhance the robustness of the analysis and give a clearer indication of the trend of the data.
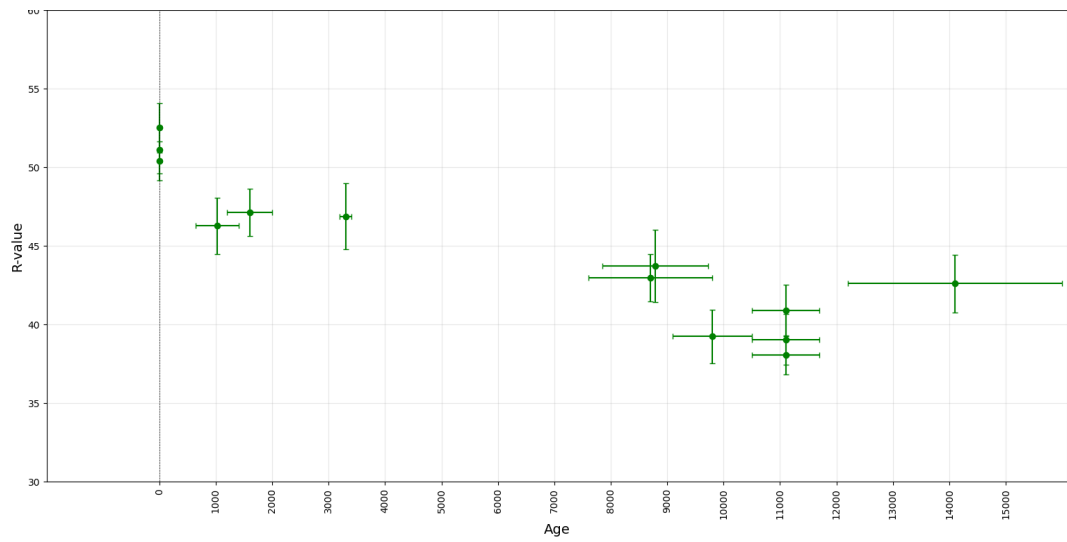
(a) Granitic ortogneiss/migmatic gneiss
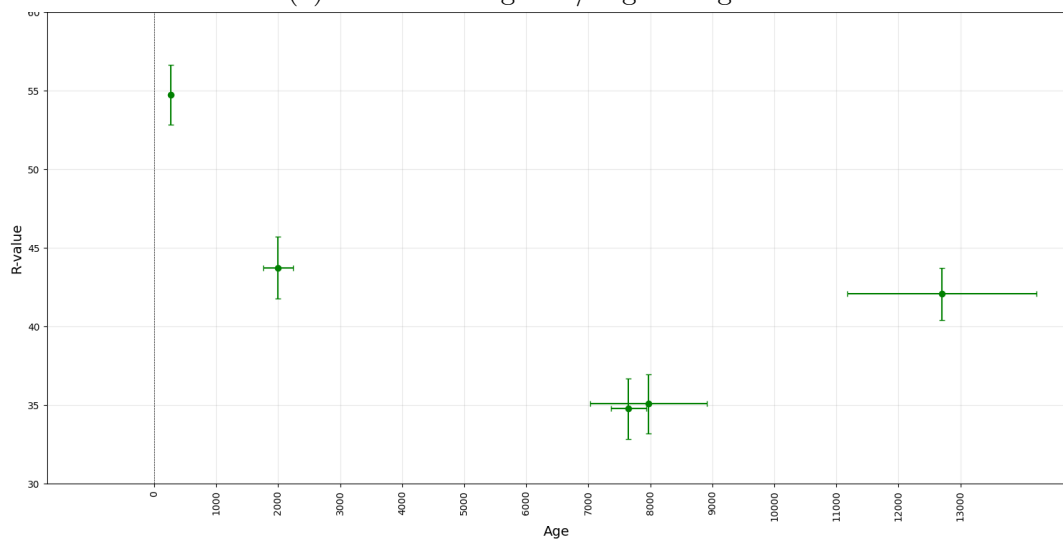
(b) Granitic gneiss/Granite
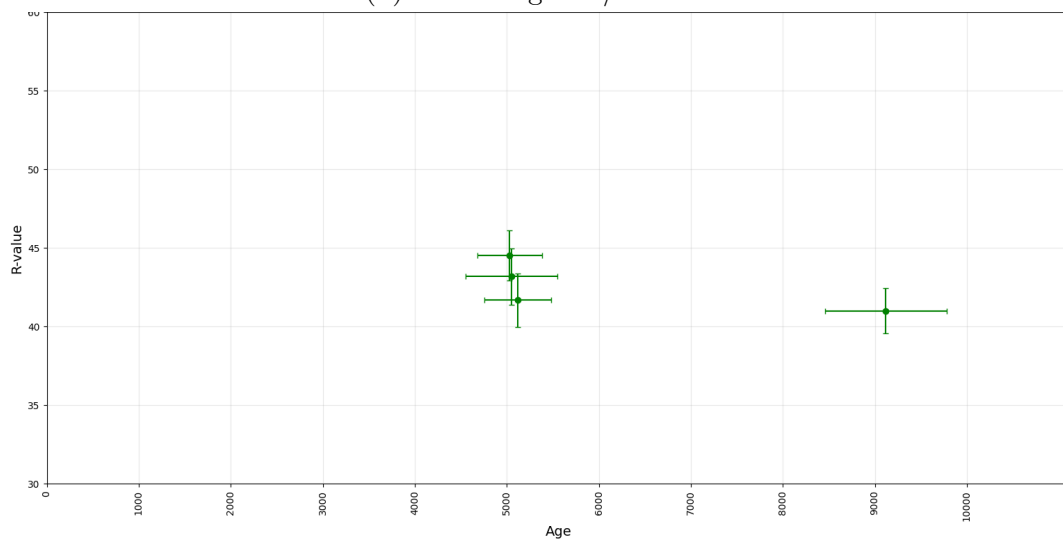
(c) Silimanitic gneiss

Figure 21: The mean and the 95% confidence intervals for the different lithological units.
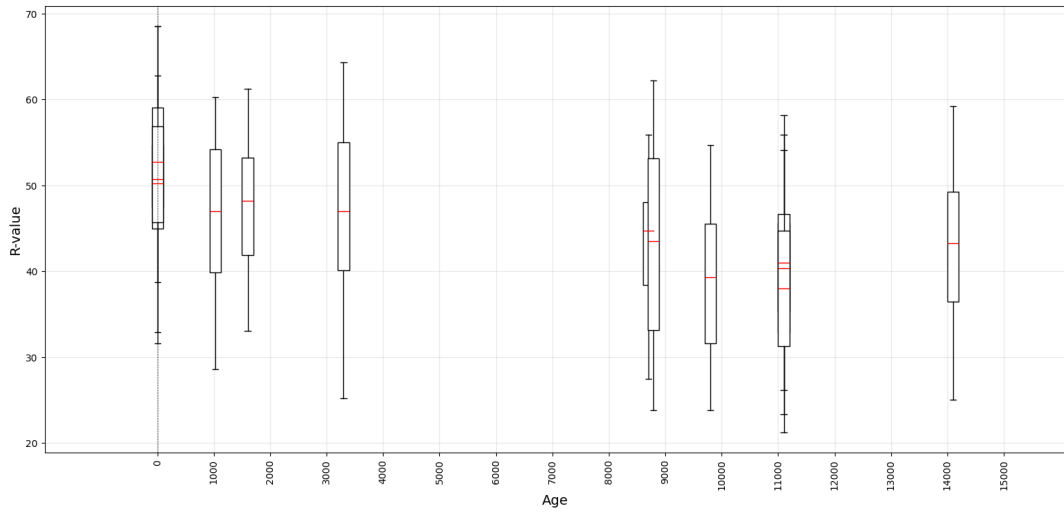
(a) Granitic ortogneiss/migmatic gneiss
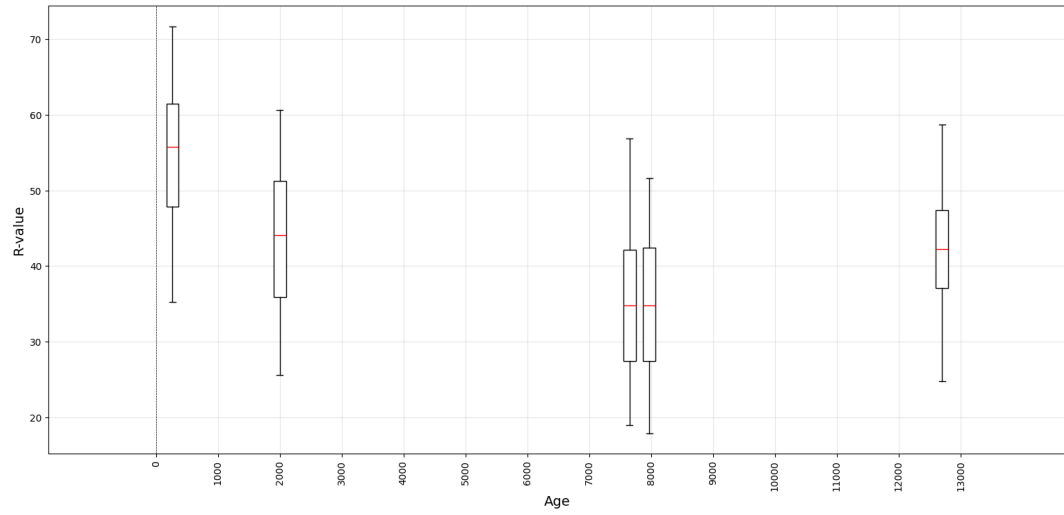
(b) Granitic gneiss/Granite
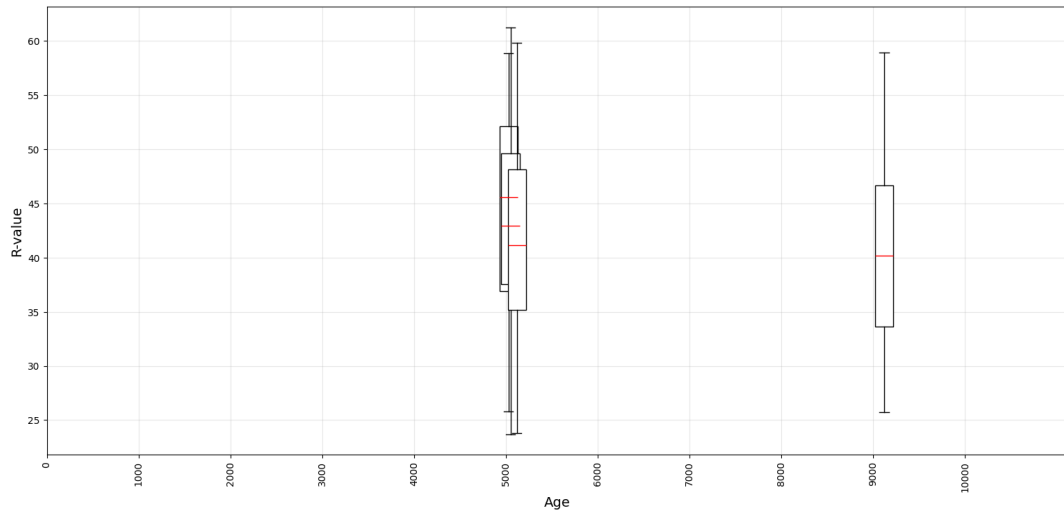
(c) Silimanitic gneiss

Figure 22: The median and the 2nd 25th 75th and 98th percentile for the different lithological units.

5.4 Kendall's τ correlation test

To test how well the data correlates a Kendall's τ test was performed. The data from the test are presented in figure 23 and figure 24.
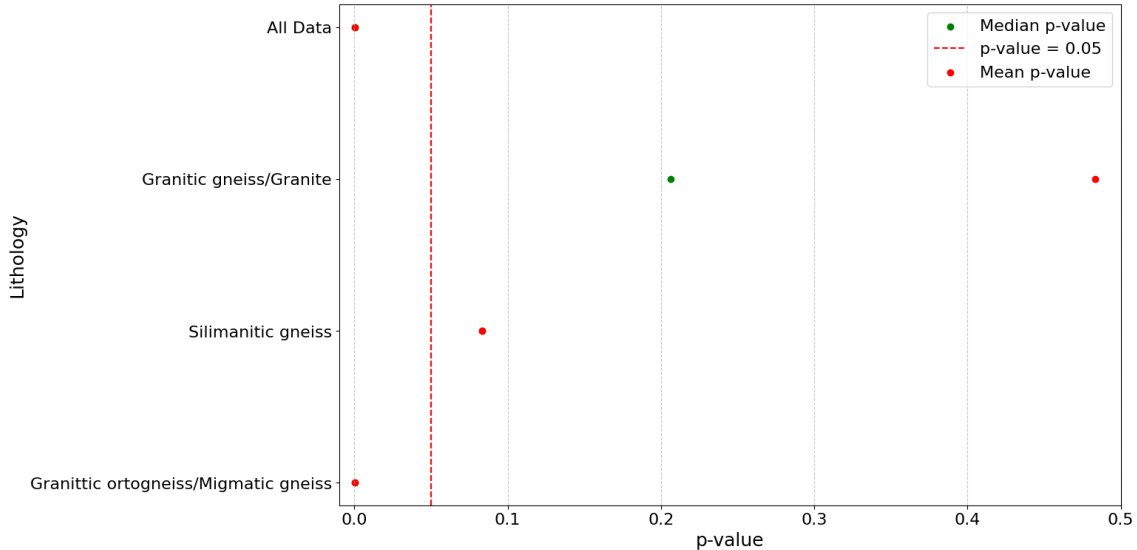
Figure 23: P-values from the Kendalls τ test. Data below the red line at p = 0.05 are considered statistically significant. Red points represent the means while the green points represents the median. For the lithologies where only one color appears, the values are equal and the points are overlaying each other.

The p-values are equal for all sets of data except for the granitic gneiss/granite-unit. Here the median has a p-value around 0.2 while the mean has a p-value just below 0.5. As both are above the 0.05-line, neither are statistically significant. The same accounts for the silimanitic gneiss-unit where both mean and median has a p-value just below 0.1. The gathering of the data from all regions and the granitic ortogneiss/migmatic gneiss-unit are both statistically significant with p-values $<<$ 0.05.

All Kendall's τ values are negative, indicating a negative trend in the data. This corresponds to a decreasing R-value by age as expected. The Silimanitic gneiss-unit has a perfect negative trend of -1, but as it contains few data points and is not statistically significant the value can not be regarded as the true value for the lithology. The statistically significant units gives a value just below -0.6 and a value between -0.7 and -0.8, where the granitic ortogneiss/migmatic gneiss has the best
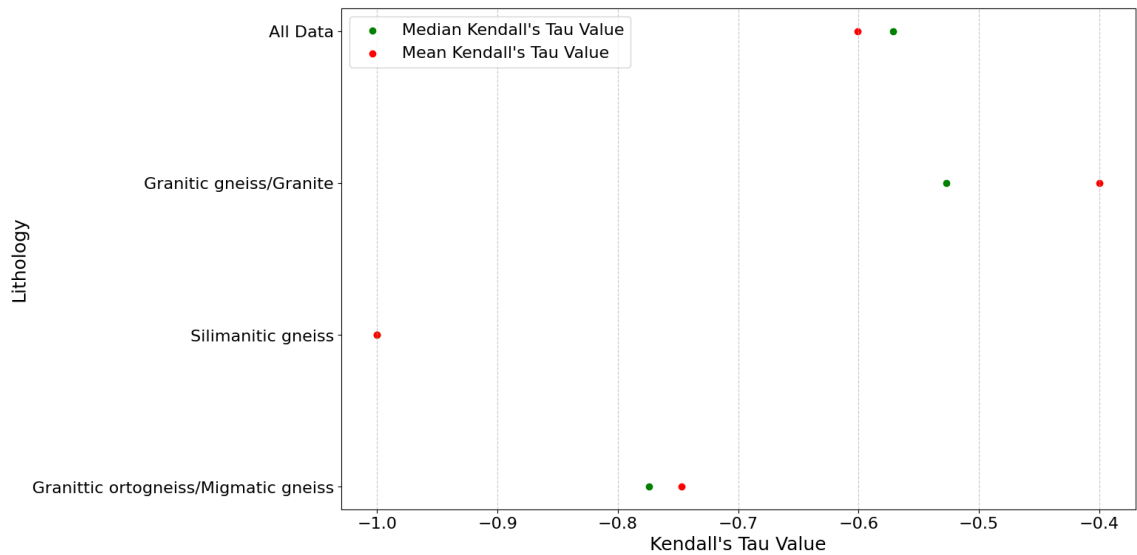
Figure 24: Kendall's τ test results for the mean and the median. Red points represent the means while the green points represents the median. For the lithologies where only one color appears, the values are equal and the points are overlaying each other.

correlation. There is a slight difference for the mean and the median. For all data the mean has a higher correlation ranking, while the opposite is true for the granitic ortogneiss/migmatic gneiss.

5.5 Alternative methods

5.5.1 The L-hammer

The results from the four calibration sites where the L-hammer was used is presented as mean and median in figure 25 and 26. As all sites lie within the same lithology, therefore, no distinction is made here.
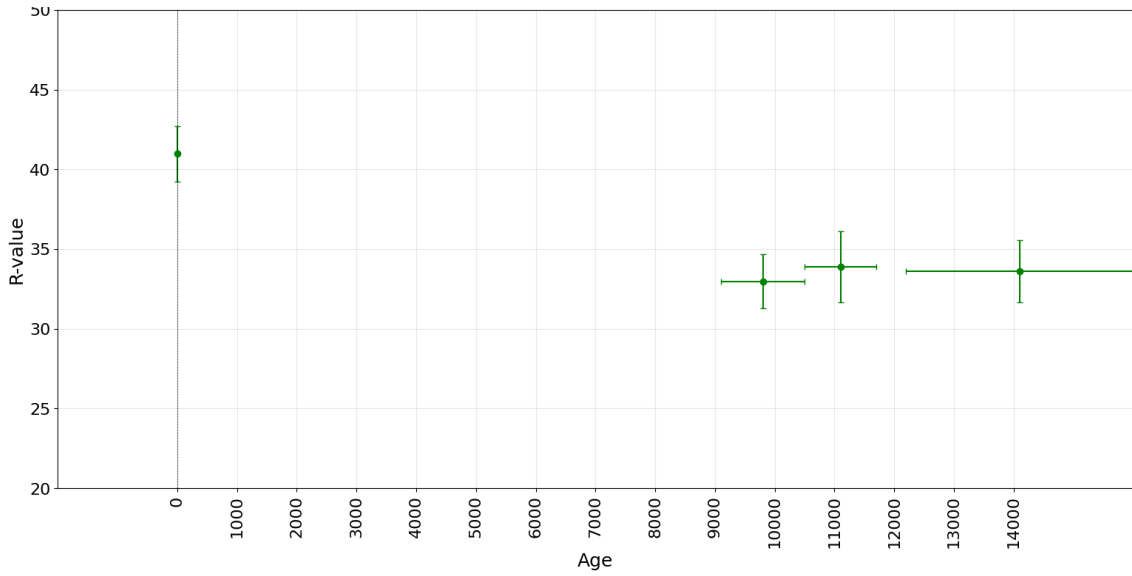
Figure 25: The mean and the 95% confidence intervals for the L-hammer on the four different calibration sites.

The R-values for both mean and median have a range between 41 and 33. This is lower than the values for the N-hammer, but the difference between the younger sites are larger than between the older. There is a decrease in R-value from the young deposits to the older ones, but the older ones do not seem to have a decreasing trend between each other. Without the single young site, the data would seem quite flat with R-values between 33-35.

A Kendall's τ test was performed on the data. This gave a correlation coefficient of -0.71 and a p-value of 0.18, which means that the data show a negative correlation but are not statistically significant.
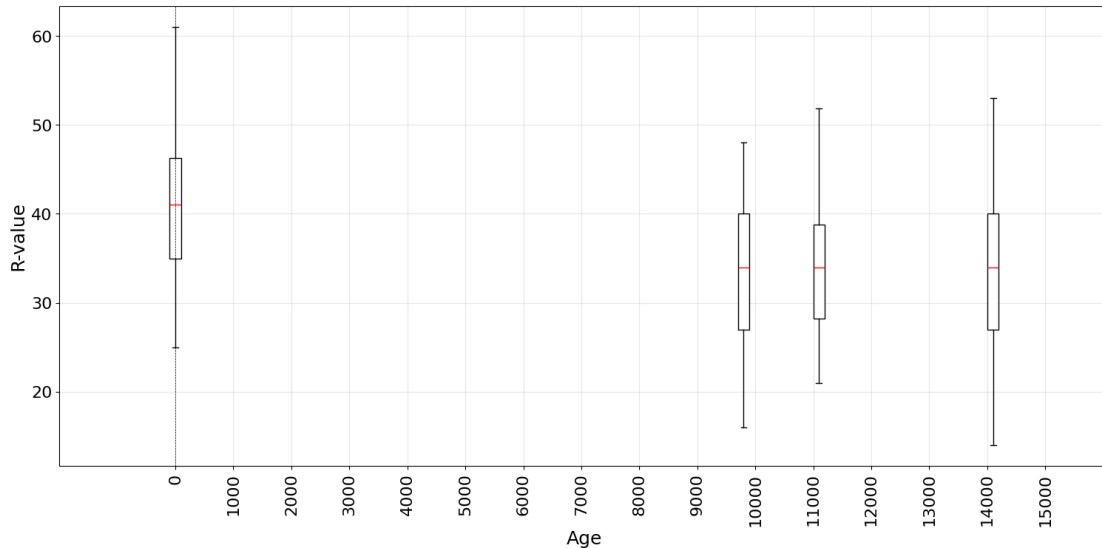
Figure 26: The median and the 2nd, 25th, 75th and 98th percentiles for the L-hammer on the four different calibration sites. Horizontal uncertainties are the same as for the mean, but are dropped to improve readability.

5.5.2 Double-hit method

The double-hit method includes impacting the same impact point twice to measure the difference when removing the outer weathering layer. Data from the test are presented in figure 27 and figure 28.

The values have a range between 5 and 12 for both mean and median. The difference in R-values seem to increase with age. This is confirmed by the Kendall's τ correlation test. The mean has a Kendall correlation of 0.56 and a p-value of 0.018 while the median has a Kendall correlation of 0.42 and a p-value of 0.09. This indicates a positive correlation where the mean has a stronger correlation than the median. The p-values indicates that the data from the mean is statistically significant while the data for the median is not.

To check if the data for the mean is valid a Shapiro-Wilk test was performed to control if the data is normal distributed. The results are presented in figure 29. The test shows that five of the sites are not normal distributed, while for four of the sites the null-hypothesis of a normal distribution can not be rejected.
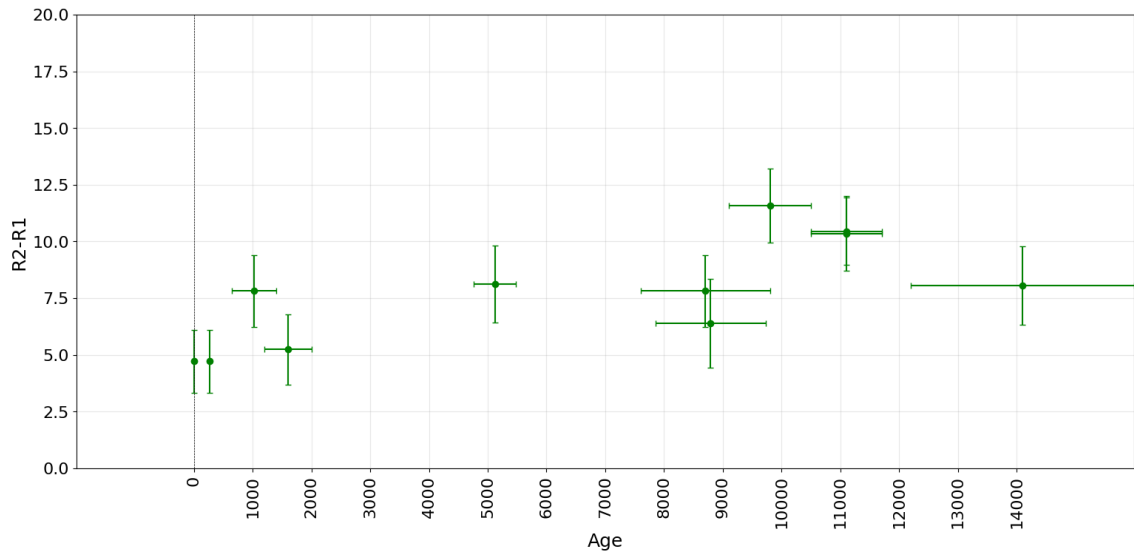
Figure 27: The mean and the 95% confidence intervals for the double-hit method.
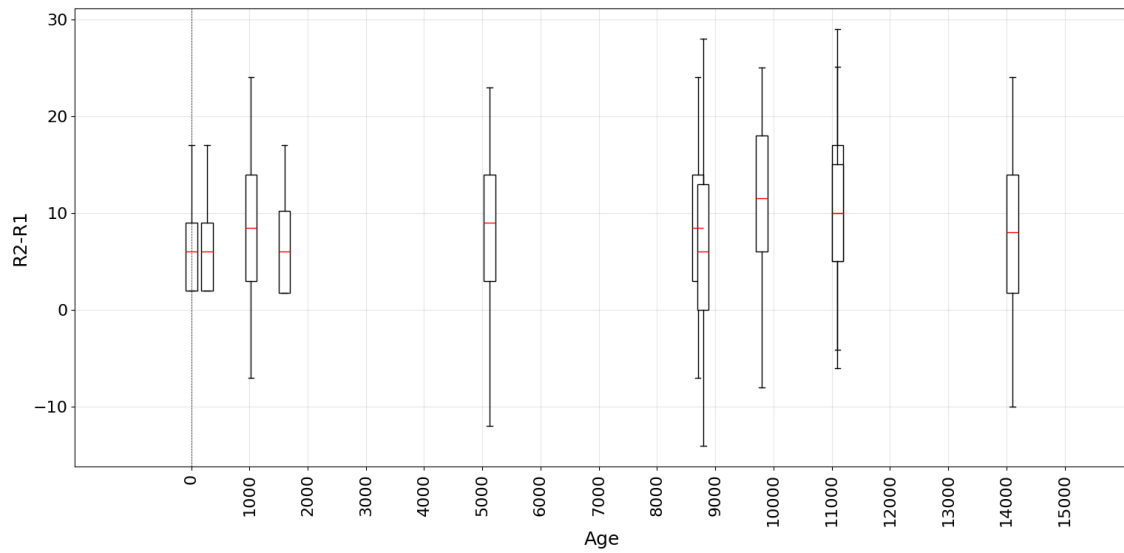
Figure 28: The median and the 2nd, 25th, 75th and 98th percentiles for the double-hit method. Horizontal uncertainties are the same as for the mean, but are dropped to improve readability.
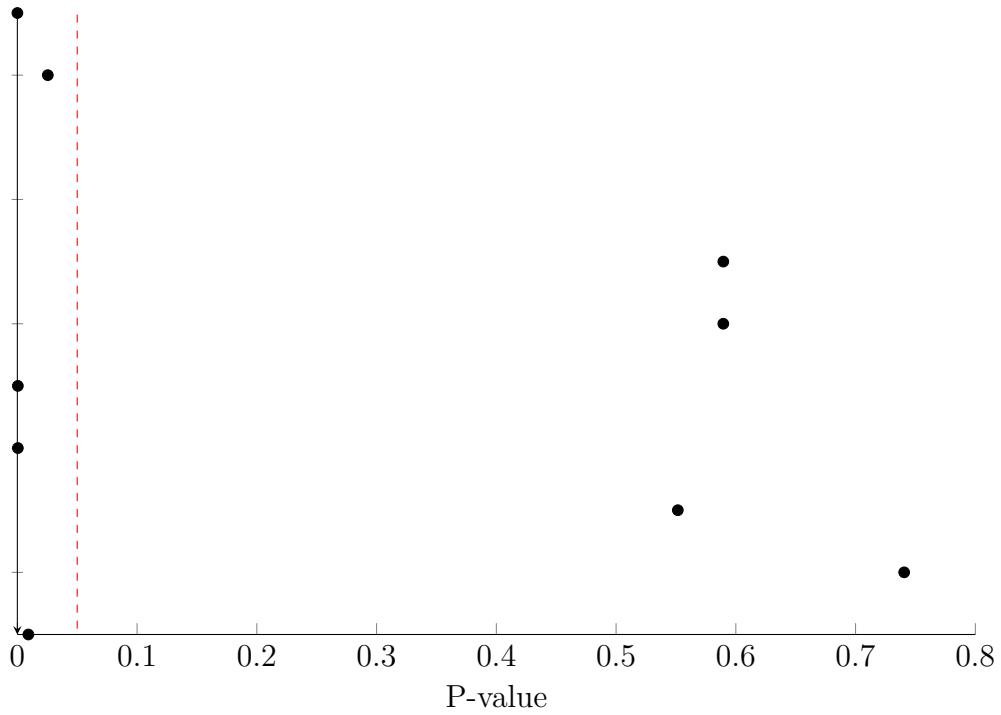
Figure 29: P-values from the Shapiro-Wilks test for each site using the double-hit method. A low p-value indicates a higher probability of a rejection of the null-hypothesis of a normal distribution. There is 95% confidence of a rejection of the null-hypothesis for values beneath 0.05.

5.6 Investigation of the method's accuracy

The results from the test of the method as described in chapter 4.4.1, based on the age and uncertainty calculation technique developed by Matthews and Owen (2010) are presented in table 5 and figure 30. To be defined as "correct estimated age" the outermost point of the uncertainty of the calculated age must be within the uncertainty of the age known from other dating techniques. The test was performed for all data combined and for the sub-lithology of granitic ortogneiss/migmatic gneiss, which showed an improved correlation and a low enough p-value to be statistically significant.

Data	Correct estimated age	Incorrect estimated age	Correct estimate (%)
All data	92	216	29.87
Granitic ortogneiss/ migmatic gneiss	43	32	57.33

Table 5: Results from the test of the method for every deposit with an age between 300 and 9000 years by every possible combination of calibration equations for calibration sites younger than 300 years and older than 9000 years, based on the age and uncertainty calculation technique developed by Matthews and Owen (2010).
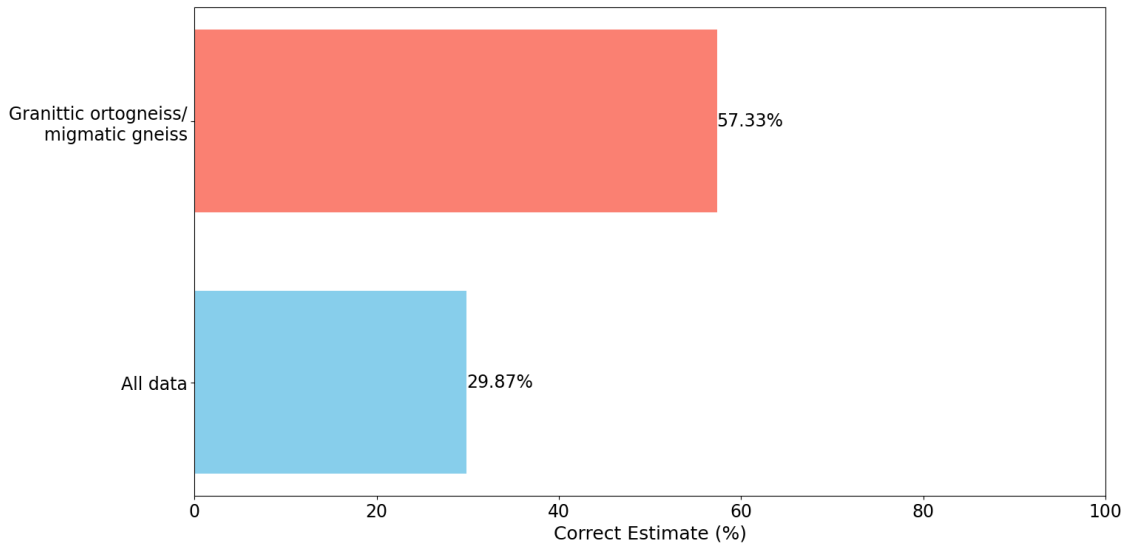
Figure 30: Bars illustrating the correct estimate percentage of the SHD-method on deposits with an age between 300 and 9000 years by every possible combination of calibration equations for calibration sites younger than 300 years and older than 9000 years.

The test gives a correct estimate for 29.87% for all the data collected and 57.33% for the granitic ortogneiss and migmatic gneiss lithological unit. Less combinations are used for the sub-lithology due to lower amount of data available.

6 Discussion

6.1 Parameters influencing the results

As described in Chapter 4.3, a number of different sources of errors may affect the results. Some of them are easy to diminish, such as avoiding moisture and using big enough rocks as sampling sites, while some are more difficult to avoid.

As gneiss is a rock composited of multiple minerals (Raade and Fossen, 2020), different responses from the hammer occurs as each impact will hit a different combination of those. The effect of different lithology was well proven by the discarded site of the hanging moraine in Innerdalen described in Chapter 5.1.1 as the quartzite gave R-values above the expectations compared to the other non-quartzitic sites. To have various mineral composition within the same site will make the spread of the R-values larger. For coarse grained rocks a solution can be to target certain minerals, but as it in nature is rarely enough homogeneity, avoidance of recognisable differences from the main lithology is imposed (Matthews and Winkler, 2021). To have a large enough number of data should also contribute to reduce the problem within a single site. A large number of R-values will thus also reduce the influence of this variation for each site. This is dependent on similarity between the different deposits, which not necessarily is the case. To have different concentrations of minerals for different locations is likely when working with heterogeneous rock and may influence the comparability of the different sites. Shakesby et al. (2006) tests the method for multiple ages for granite, a more homogeneous rock type. Their results gives a plot with a strong linear trend compared to the results in this study. This may indicate that the inhomogenity of gneiss has a great influence in the large spread of the R-values at each site (see appendix B).

To diminish the effect of the difference in lithology between the sites, the gneiss in the study area was divided into sub-lithological units based on the bedrock map by NGU, utilizing the most detailed mapping scale available (Chapter 5.3). Of the three sub-lithologies only granitic ortogneiss/migmatic gneiss contained enough data to be statistically significant with a P-value 0.009. The Kendall's τ value for the mean

was -0.75. This proves a stronger correlation than for the combined data from the different lithological units, and may therefore indicate a possibility of the difference in lithology affecting the results.

The micro roughness of boulders formed by failure processes is pronounced. It was aimed to not hit big outstanding points on the rocks, but as many rocks contains unevenness on a smaller scale on the whole surface, the influence of the roughness is not possible to avoid. The use of deposits made by the same processes (rock slope failures) for all study sites is the best approach to have the relative same amount of irregularities affecting the results (Matthews and McEwen, 2013; Matthews and Winkler, 2021).

The drift of the hammer which occurred over time may also have an effect on the data. To diminish this influence only values of high accuracy was accepted, with a standard deviation less than ± 2 on the anvil test. Still some anvil test values were below what is recommended from the manufacturer (Proceq, 2002). This should be considered while analysing the results. Figure 31 compares the sites where the anvil test was within the recommended standard with the sites where they were below but with a good consistency.
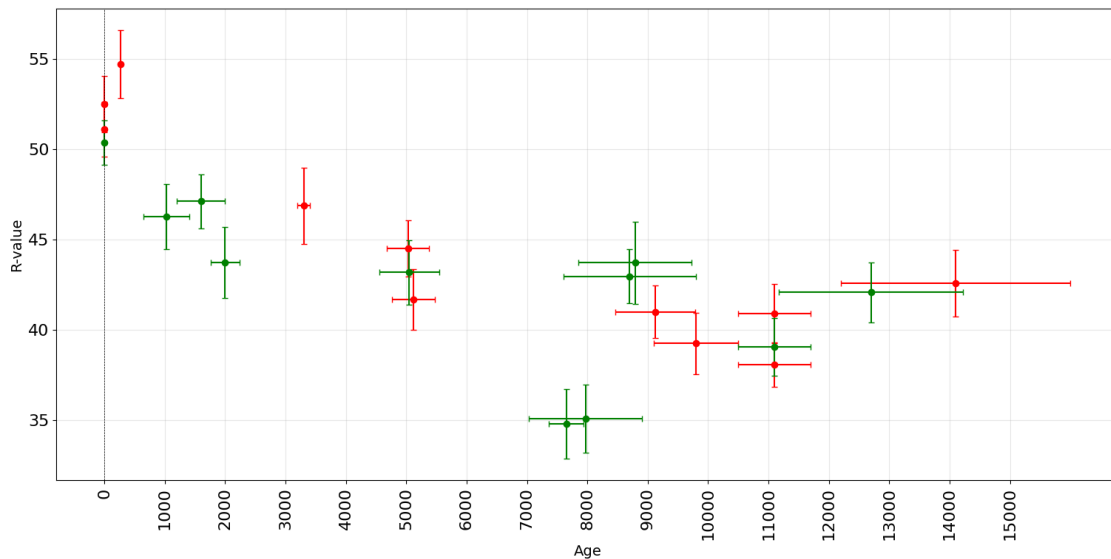
Figure 31: Comparison of the sites where the anvil test gave values within the recommended standards (Green points) and where it gave values below the recommendations, but with high consistency (Red points)

While the trend looks more or less similar, some differences are apparent. The youngest deposits seem to have a higher R-value with an anvil test below the recommended standard. To determine if this is a permanent difference or just randomness in the data would require more data. The two sites with the lowest R-values from Innerdalen seems to differ from the rest of the data. As they are green, these outlying values are not produced by a fluctuations of the Schmidt hammer as tested by the anvil calibration.

A Kendall's τ test was performed on the two different sets of data. For the values within the recommended standard the Kendall's τ value was -0.53, while for the values below the recommendations the Kendall's τ was -0.69. Both of the p-values $<<$ 0.05 so that both can be regarded as statistical significant.

The drift may have had an influence of significance on the data, and should be regarded as a potential source of error. Since the data correlate well in the comparison and no significant differences are observed between the values within and below the recommendations, it is assumed for the remainder of the analysis that this does not critically impact the data.

6.2 Calibration site analysis

There seems to be a trend when comparing the R-values to the age of the independently dated deposits, where the R-value decrease by the age of the deposit. This corresponds well with former findings (E.g.: Nesje et al., 1994; Aa et al., 2007; Matthews and Owen, 2010; Wilson et al., 2019). Taking into account the whole range of values in table 16 and 19 it is apparent that the R-values do not result in a perfect linear relation with independent deposit ages, and multiple values depart from a straight line. This is also tested by the Kendall's τ correlation factors in figure 24. The test confirms a negative correlation, but not a perfect decreasing linear trend.

Some outliers may influence the overall impression of the data. The two sites in Innerdalen with an age just below 8000 years shows particularly low R-values compared to trend of the other sites. The hammer was within the recommended anvil calibration values as demonstrated in figure 31 and no abundance of irregularities or

difference in lithology compared to other sites were detected during the field work. The site measurements were taken later in the evening on a particularly cold day, proved by frost in the grass and on some rocks the following morning. As the use of the hammer is not well studied in different temperatures, this observation does not lead to any conclusions.

The oldest deposits of Gråura and Setra surprisingly have a higher R-value than the deposits slightly younger. This gives an impression of a better fit of an exponential curve. The possibility of an non-linear curve has been explored in previous publications (Stahl et al., 2013 ;Tomkins et al., 2018), but for surfaces in the Holocene timescale a linear trend is considered the most precise correlation trend (Shakesby et al., 2011; Matthews and Winkler, 2021).

6.3   Mean versus Median

The Shapiro-Wilk test for normality proved how some of the data are not normal distributed. A look at the histograms in Appendix B confirms how a number of the R-values per site do not follow the normal distribution pattern illustrated in figure 2. The varying adaption to a normal distribution is not unique for this study. From former research where histograms are presented it is apparent how some data may replicate a normal distribution (Nesje et al., 1994; Matthews and Owen, 2010; Matthews and McEwen, 2013; Marr et al., 2019; Matthews et al., 2019), while a lot of data also fails to show such an adaption (Matthews and Winkler, 2011; Matthews et al., 2015; Matthews et al., 2017; Matthews et al., 2019; Då, 2020). All of these studies are also performed on gneiss.

As an approximated normal distribution is required for the mean and confidence intervals to be applicable (Løvås, 2018), the certainty of the mean as a tool in the Schmidt hammer dating method should be questioned.

The disparity between the mean and median values is small (Figure 20). The largest difference arises in their respective uncertainties as the mean is characterized by 95% confidence intervals based on the standard errors while the median applies different percentiles, resulting in larger uncertainties. For the Schmidt hammer

dating method to be as useful as possible, small uncertainties are preferred. However, if the uncertainties from the data becomes too small for the true age to stay within the estimated age interval, it compromises the integrity of the method.

6.4   Other publications

A number of former studies applies the Schmidt hammer dating technique in their research. To investigate if the data from this study has the same characteristics, a comparison was performed. All of the studies listed in figure 32 are performed on gneiss in Norway, south of Trondheim. The mean is used for the comparison as this is what is the given value in the publications.
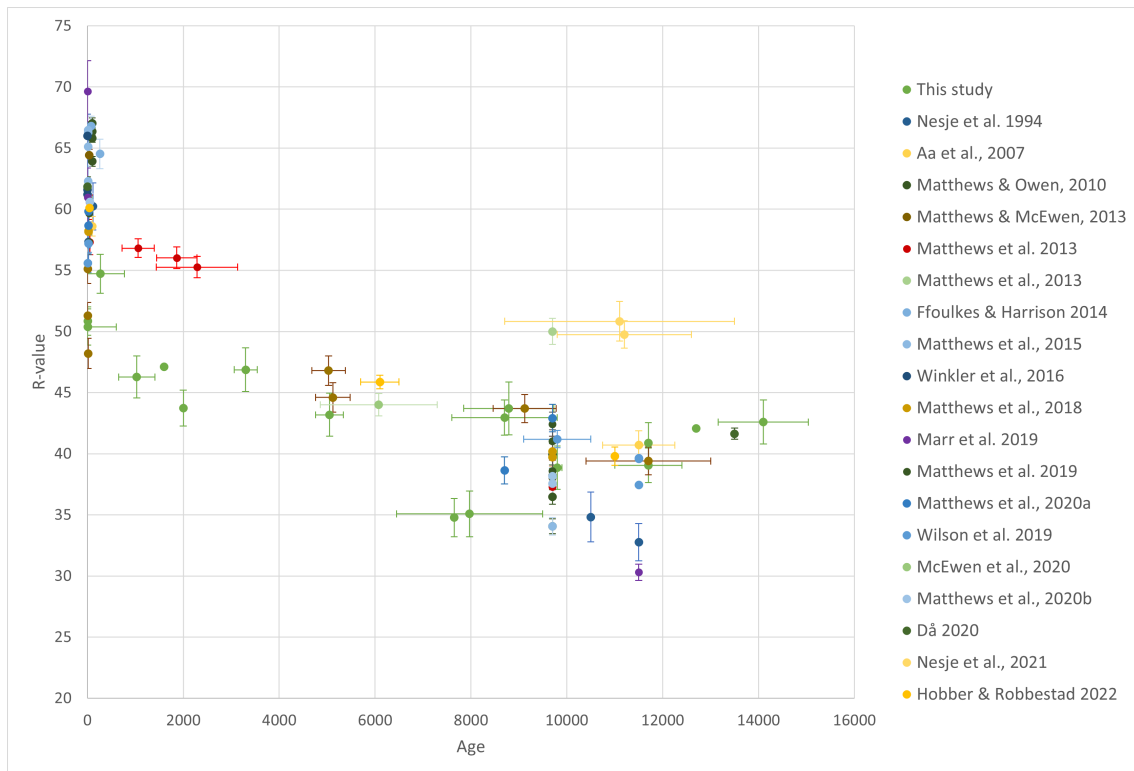
Figure 32: Data for all former studies performed on gneiss in southern Norway.

Figure 32 shows a very large spread of R-values for different ages. Still a decreasing R-value with age is apparent, but not with a perfect linearity. To compare this data would require an assumption of characteristics similar enough for the weathering rate to be the main influence on the R-value. This is not necessarily true, as the collection of data belongs to a wide geographical region. Therefore a full analysis of

the data collected may not be useful, but a overview on how much influence different parameters potentially have is apparent.

Differences between studies within the same study area or of proximal geographical location also exists. For example in the master thesis by Då (2020) a calibration equation was developed, but as it was a mismatch to the one already developed in the area by Matthews and Wilson (2015) it was decided to use their calibration equation instead. The study area of Matthews et al. (2014), Matthews et al. (2019) and Matthews et al. (2020a) overlaps each other and is within the same lithological unit. The three calibration equations established prove to be significantly different from each other (table 6).

Publication	Calibration equation
Matthews et al. 2014	25149.369 – 414.41441x
Matthews et al. 2019	31067.911 - 520.749x
Matthews et al. 2020	34222.704 - 571.66479x

Table 6: Calibration equations from three different studies with overlapping study areas

This proves how a great variability already exists in the method.

6.4.1 Lithology

In chapter 5.3 it was found how sub-division into sub-lithologies of the gneiss could improve the correlation of the data. Matthews et al. (2018) argues how the difference in lithology will have a small impact compared to the weathering effect in the Holocene timescale. A sub-division can still be performed for the data from the publications for comparison. The sub-dvision is based on descriptions by the authors and the bedrock map of NGU (Figure 9) and is demonstrated in figure 33

The granitic ortogneiss/migmatic gneiss still seems to have the same large spread of R-values, while the granitic gneiss/migmatic gneiss seems to be slightly more linear, however with significantly less data. The pyroxene granulite gneiss clearly has the most linear trend. It has very large concentrations of young control sites and sites
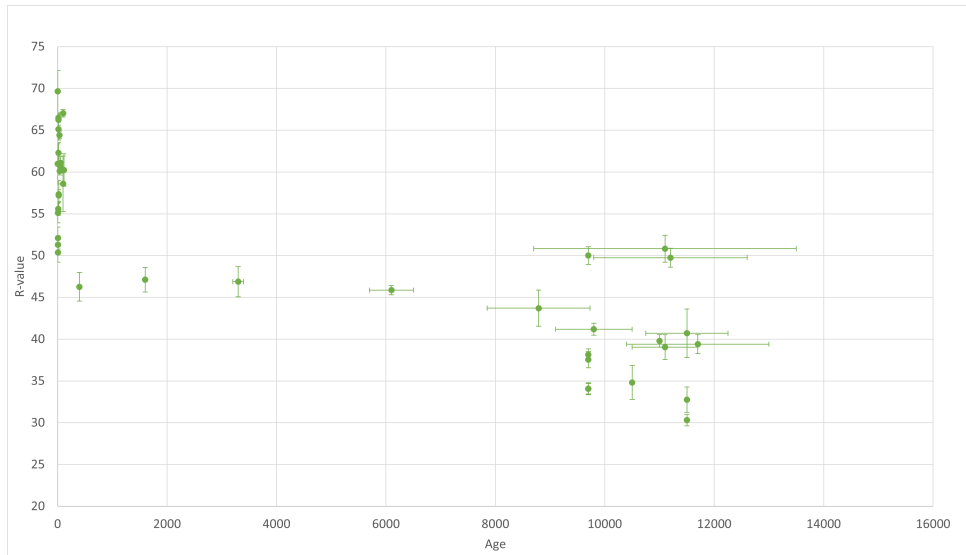
(a) Granitic ortogneiss/migmatic gneiss
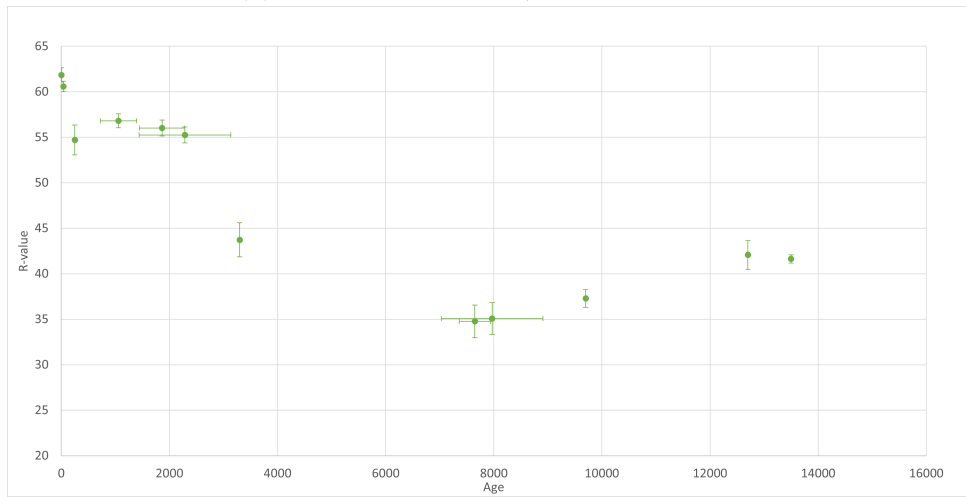
(b) Granitic gneiss/Granite
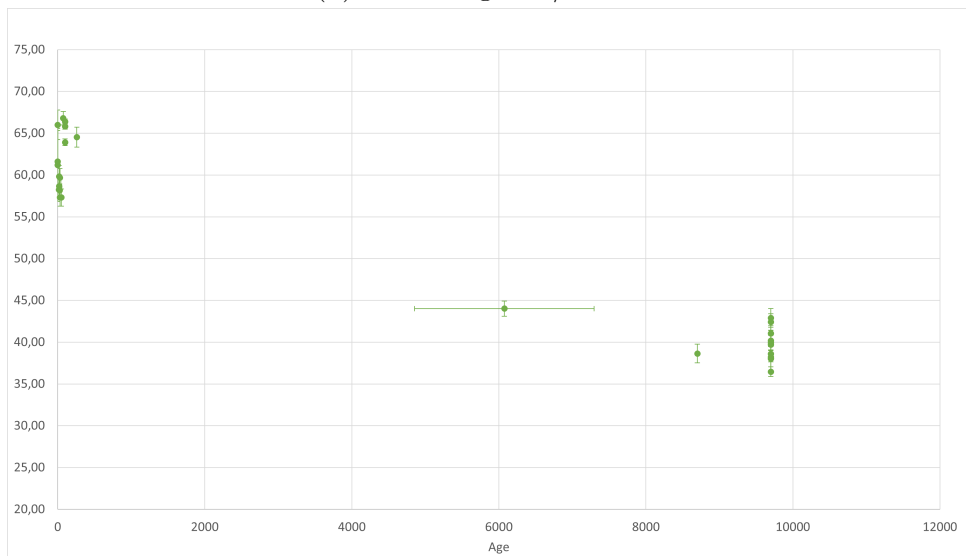
(c) Pyroxene granulite gneiss

Figure 33: The mean and the 95% confidence intervals for the different lithological units for all studies in southern Norway.

a bit younger than 10 000 years old. This is a result of multiple studies performed by the same main author in one area over a long period in time, producing multiple publications (E.g.: Matthews and Owen, 2010; Matthews et al., 2020a). Moraines and glacially scoured bedrock with an assumed age of 9700 years were used as old calibration sites. The spread of the R-values for these sites are significantly lower than for the two other lithologies, where a more diverse group of authors are involved. This may indicate that different operators may have an influence on the R-values.

6.4.2 Young control sites

It is noticeable how the sites with youngest ages have some of the largest spreads of R-values relative to each other (Figure 16, figure 19 and figure 32). Surfaces produced by different processes for the younger surfaces have been used, where the difference in roughness may have an effect on the R-value (Matthews et al., 2018). To compare the different surfaces used as younger calibration sites, they have been separated into four different categories in figure 34.
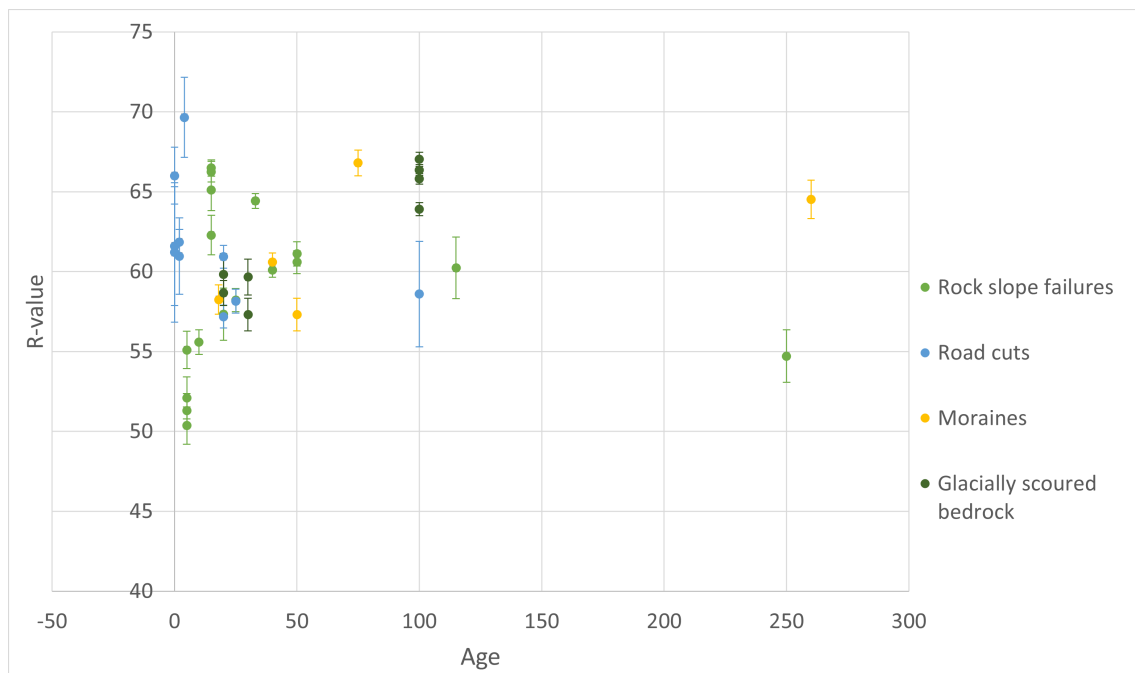
Figure 34: Types of young control sites used for the different studies.

The glacially scoured bedrock is expected to have a higher R-value as the roughness is lower due to their polished surfaces (Matthews et al., 2018). In the same

paper it is also discussed how road cuts should inherit the same qualities as fresh rock slope failures as the roughness is similar. In figure 34, the glacially scoured bedrock appears to have higher R-values compared to the rock slope failures and moraines. Also the road cuts seems to have relatively high R-values. Rock slope failures comprises multiple episodes of movement pre-failure where cracks are opening (Hermanns et al., 2022). This may lead to pre-exposure to weathering of the rocks before the time of the failure, which may explain the lower R-values of the rock slope failures compared with road cuts. This could also be an explanation to the bi-modal distribution of some of the histograms in appendix B.

6.5 Alternative methods

6.5.1 The L-hammer

A small amount of data were acquired for the test of the L-hammer. The correlation corresponds to the correlation of the N-hammer according to the Kendall's τ test, but are not statistically significant. The three older deposits do not seem to have a decreasing R-value with age. It could be speculated if the L-hammer is unable to detect differences between lower R-values for hard rocks, but it would require more data to reach a conclusion.

6.5.2 Double-hit method

The method of hitting the same spot twice has, as opposed to the traditional SHD method, a positive correlation trend. The idea was initially proposed by Aydin and Basu (2005) as a potential alternative method of measuring degree of weathering. Any prior attempt of rock dating by this method has not been performed. The idea is that the higher the degree of weathering, the larger is the difference between the first and second impact. This corresponds well with the increase of the difference in R-values by age. The correlation is, according to the Kendall's τ test, close to, but a bit lower than the traditional method. This proves that the method has potential within rock surface dating and could be further explored.

6.6 Accuracy of the method

The Schmidt hammer dating technique has through recent advances been called a high-precision dating technique (Shakesby et al., 2006; Matthews and Owen, 2010; Matthews and Winkler, 2011; Matthews and McEwen, 2013; Marr et al., 2019) and Wilson et al. (2019) suggest it is of comparable accuracy and may have improved precision over ^{10}Be-ages. Shakesby et al. (2011) proves how well the method works on granite surfaces over a great range of various ages.

The test performed in chapter (5.6) may suggest a lower accuracy for the method on gneiss than formerly proposed. If data from all test sites is included, only 29.87 percent of the ages tested were correctly estimated. This number is increased to 57.33 for the granitic ortogneiss/migmatic gneiss sub-lithology. This increase in precision corresponds well with the higher correlation value according to the Kendall's τ correlation test. The correct estimate percentage is relatively low for both tests, as neither a 30% or 57% chance of the true value being within the uncertainty margins are very impressive for a high-precision method.

6.7 An attempt to develop a new method

As the accuracy of the method with the applied uncertainties is not satisfactory, alternative methods of using the data can be discussed. There is a proven trend of a decreasing R-value with an increasing age, but some issues appear by using it as a dating method for surfaces in gneisic lithologies of an unknown age. The main problems seem to be:

1. A lack of a strong enough linear correlation to determine the ages between a young and old control site within the calculated uncertainty limits.

2. A large number of data not appearing as normal distributions, making the applicability of the mean and confidence intervals assuming a distribution of the data less reliable.

To counteract these issues, an attempt to make a new method for Schmidt hammer dating was made. This method is based on the median and the percentiles of the R-values from each site, trying to extend the uncertainty limits to a more trustworthy range. Figure 35 demonstrates the principles of the new proposed method.
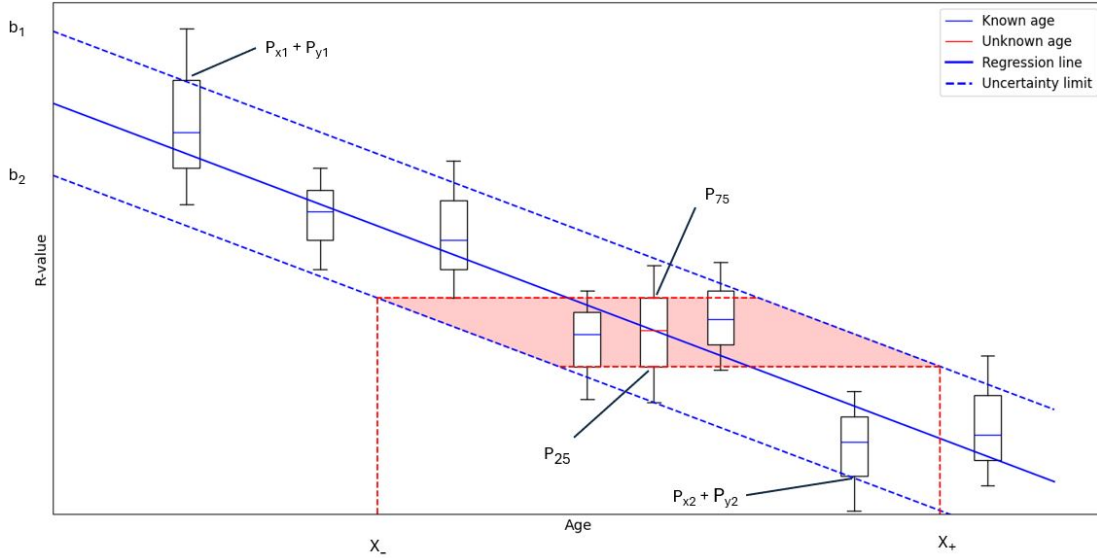
Figure 35: Illustration of the proposed new method. The red area represents the age range for the deposit with an unknown age.

This method applies the median, 25th and 75th percentile of multiple sites with a known age. The calibration equation is based on the regression line between these sites, and the age value can be determined by the equation for a straight line. Keep in mind that this equation is used when the age is on the x-axis as presented in the results of this study. Application on data with age on the x-axis would have to change the formula accordingly.

$$x = \frac{y - b}{a} \tag{14}$$

where x is the age, y is the R-value of the site with an unknown age and a and b are the slope and constant value for the regression line through the medians.

To determine the uncertainties, two different lines parallel to the calibration line are drawn. The upper line has a fixed point at the 75th percentile furthest away from the calibration line, while the lower line has a fixed point at the 25th percentile with

the same characteristics. These lines acts as uncertainty lines. The constant b-value for the uncertainty lines can be found by substitution in the calibration equation:

$$b = P_y - aP_x \tag{15}$$

Where P_x and P_y are the x and y-value of the respective 25th or 75th percentile and a is the slope of the calibration line.

We also need to consider the uncertainties of the R-value for the deposit we want to date. Therefore we add these into the equations, and extend the uncertainty limits from the 25th and 75th percentiles of the unknown deposit along the x-axis until they reach the uncertainty lines. This would make up an area of uncertainty. The positive and negative uncertainties will be different due to the nature of this method, and can be found according to the formulas:

$$X_+ = \frac{P_{25} - b_u}{a} \tag{16}$$

$$X_- = \frac{P_{75} - b_l}{a} \tag{17}$$

Where X_+ and X_- are the positive and negative age uncertainty, P_{25} and P_{75} are the 25th and 75th percentiles for the R-value of the site we want to date, b_u and b_l are the constants where the upper and lower calibration lines intersect the y-axis, and a is the slope of the lines, which is the same for the calibration line and the uncertainty lines.

The method was applied for the undated sites illustrated in figure 8. The results are presented in table 7.

Site	Estimated age	Uncertainty (+)	Uncertainty (-)
Isfjorden	10000	19500	23400
Remmem	11800	18900	25000
Tomberg	11400	20500	26400
Alstadfjellet undated	12100	18000	24300
Gravemsura	9700	19100	26200
Mona	10200	18700	23700
Mardalen	10300	18700	25700

Table 7: Dating of the deposits of an unknown age applying the suggested new method of Schmidt hammer dating. Values are rounded to the closest 100 years.

The result from the method shows that all of the sites has ages in the close range between 9700 and 12100 years. This corresponds well with their close R-values listed in appendix D. The uncertainties are very large. This is the consequence of the large spread of the data for each deposit and the non-perfect linear correlation between the sites. As the lithological sub-division showed an improved correlation, an attempt to use the method for deposits within the Granitic ortogneiss/migmatic gneiss sub-lithology was performed to see if the uncertainties would decrease. The results are presented in table 8.

Site	Estimated age	Uncertainty (+)	Uncertainty (-)
Isfjorden	10700	18700	18200
Remmem	12700	18000	20000
Tomberg	12200	19700	21400
Alstadfjellet undated	13000	17000	19200
Mona	10900	17700	18500

Table 8: Dating of the sites in the granitic ortogneiss/migmatic gneiss sub-lithological unit applying the suggested new method of Schmidt hammer dating. Values are rounded to the closest 100 years.

The dates from the sub-lithology give higher ages and lower uncertainties. Still the uncertainties are very large, and indicates no more than how the rock slope failures occurred approximately sometime during the last 30 000 years. This does not provide useful information, and like for the original method, the proposed method can not be recommended to use for rock slope failures in gneiss.

The issue for the data in this study, as demonstrated in chapter 5.6, is that the Schmidt hammer dating method has a relatively low probability of accurately estimating the correct age. The proposed new method does increase the uncertainties, but these become too large for any meaningful interpretation. Reducing the uncertainties further would require excluding more data. However, since the current method already uses the 25th and 75th percentiles, effectively including just 50% of the data, further exclusion would risk excessive data manipulation. This would make the data fit the desired outcome without any statistical justification.

An argument could be to use the data for relative dating, as a trend of a decreasing R-value by increasing age is apparent and has a correlation. Therefore it could be formulated as the deposit in Isfjorden (Median R-value: 41.2) is younger than the deposit at Skiri (Median R-value: 39.3, age: 11700) and older than the deposit at Venja (Median R-value: 48.2, Age: 1600). The wording of *probably* is important as the data is too uncertain to be conclusive.

The proposed method uses multiple points and therefore removes some of the advantages of the original method as a quick and easy applicable method. The lower number of points used, the higher is the probability of a result with low uncertainties due to the lower probability of an extreme point affecting the outcome. This further weakens the usability of the method as more work is required to collect enough data and a few data points may not be sufficient.

6.8 Timing of the rock slopes failures compared to the glacial retreat

With enough deposits with a known temporal distribution, we are able to compare the timing of the rock slope failures with the time of glacial retreat. This comparison can provide a wider understanding of the triggers of large rock slope failures in glaciated and former glaciated regions.

The comparison was performed with deposits dated by TCN, radiocarbon and historical events, in addition to the SHD-dating provided by this study. As the results of this study proved to be unreliable using the traditional SHD-method, ages with uncertainties from the method developed in chapter 6.7 was used. The applicability of these dates is questionable due to their large uncertainty range and should be reflected upon when analyzing the figure. They are still chosen over the traditional method as it was proved a very low accuracy for this technique on the data from this study. Therefore it was considered more representative with a method that shows how uncertain the data could be, instead of giving low uncertainty estimates with a high probability of being inaccurate. The uncertainties for the SHD-dates are simply set as >15 000 years, as the age can not be negative and the probability for the deposits being older than 15 000 years is low due to the removal of material by the glaciers. The calculated uncertainties can be found in table 7 and table 8.

Figure 36 shows how the probable temporal distribution of rock slope failures is spread out after the glacial retreat (Hughes et al., 2015; Romundset et al., 2023). One limitation of this map is how the deglaciation lines fits well with the valley floors, but mountain tops have been melting out of the ice prior to the suggested lines that are based on valley deposits.

A number of events seems to be concentrated close to their respective timing of deglaciation. This is an indication on how the removal of glacial support may contribute to destabilization and rapid collapse of rock slopes (Kos et al., 2016). An alternative hypothesis is that seismic activity was stronger due to high rebound rates following deglaciation (Anda et al., 2002). This activity might have been a trigger for rock slope failures shortly after glacial retreat.
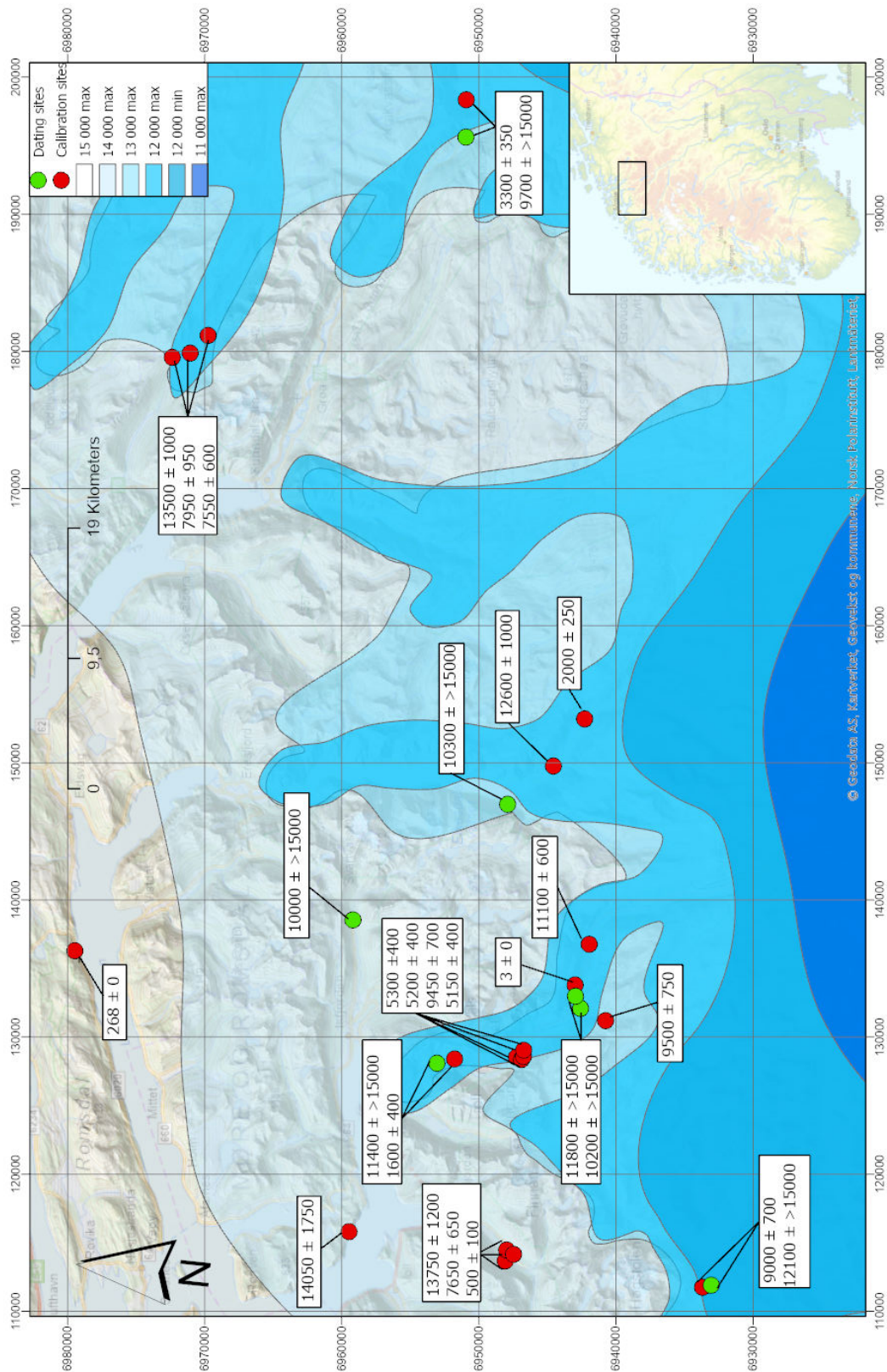
Figure 36: Map of all deposits and their ages compared to the deglaciation time of the valleys. The blue-colored areas represent ice cover for different periods according to the Dated-1 database from Hughes et al. (2015) and Romundset et al. (2023). The extent of the glaciers is extrapolated over the higher altitude areas and is therefore not accurate outside of the valleys.

A smaller cluster of deposits also falls within the limits of the Holocene thermal maximum (8000 - 5000 years ago). This corresponds with the work of Marr et al. (2019), where a higher number of rock slope failures are found to occur during this period. Hilger et al. (2021) suggest how permafrost can have a stabilizing effect over several millennia after deglaciation. These results confirms the possibility for this, but the probability of the rock slope failures still seem to be highest shortly after glacial retreat.

These findings indicate that a warmer climate contributing to the melting of glaciers and permafrost degradation may cause a larger number of large rock slope failures. The warming climate caused by human activity may therefore contribute to increasing the frequency of rock slope failures. Extra attention should be directed towards glaciated areas with a retreating glacial extent and areas where permafrost degradation can occur.

7 Conclusions

The study investigated the accuracy of the Schmidt hammer dating method on large rock slope failures in gneiss through statistical analysis and comparisons with already dated deposits. A development of a new method was proposed, and a comparison of the temporal distribution of large rock slope failures and timing of deglaciation was investigated. The key finding were:

- The rebound of the hammer is inversely proportional to the age of the deposits. However, there is not a perfect correlation, and a large number of factors have the possibility to influence the rebound value. The degree of weathering caused by the exposure time of the surface may be the main contributor to the reflected surface hardness, but the noise created by other influences such as roughness of boulders resulting form rock slope failures, weathering prior to failure, and mineral heterogeneity seem to highly disturb the correlation.

- Lithological variation within the gneiss between granitic gneiss/migmatic ortogneiss, granitic gneiss/granite and silimanitic gneiss is proven to have an effect, and the suitability of the Schmidt hammer exposure age dating method on gneiss seems questionable according to the data of this study. As it is proven a strong correlational trend in former studies of the method in pure granite, the nature of the gneiss may be the cause of the low reliability for the method in this study. Data from some other studies performed on gneiss also shows a large spread in the quality of the results.

- The Schmidt hammer exposure age dating method proved to have a low accuracy for the data in this study, and the distribution of the data sets did not fulfill the requirements to use some of the statistical parameters of the SHD method. A proposal of a new method based on medians and percentiles for a larger set of data was developed. The resulting uncertainties from this method was too large for any meaningful interpretation and the method can therefore be considered a failure for the data in this study. More research and testing on other data sets and further development of a new method could be performed in future research.

- The temporal distribution of the rock slope failures clusters around, but not exclusively, two periods: close to the time of deglaciation and during the Holocene thermal maximum. Therefore it is assumed that a warmer climate has increased rock slope failure activity, due to permafrost degradation and retreating glaciers, followed by seismic triggering due to rapid isostatic rebound.

One additional finding were noted during the research:

- To perform two impacts on the same location of the rock to measure the difference in rebound show a promising trend in surface age dating. Further investigations could be performed.

References

Aa, A. R., Sjåstad, J., Sønstegaard, E., & Blikra, L. H. (2007). Chronology of holocene rock-avalanche deposits based on schmidt-hammer relative dating and dust stratigraphy in nearby bog deposits, vora, inner nordfjord, norway. *The Holocene*, *17*, 955–964. https://doi.org/10.1177/0959683607082411

Agresti, A. (2010). *Analysis of ordinal categorical data.* Wiley Series in Probability; Statistics (Second ed.), John Wiley & Sons.

Anda, E., Blikra, L. H., & Braathen, A. (2002). The berill fault-first evidence of neotectonic faulting in southern norway. *Norsk Geologisk Tidsskrift*, *82*, 175–182.

Austigard, B. (2016). Digerura i eikedalen - omkring ei datering. *Naturkatastrofer*, 121–143.

Aydin, A., & Basu, A. (2005). The schmidt hammer in rock material characterization. *Elsevier, Engineering Geology 81*, 1–14. https://doi.org/10.1016/j.enggeo.2005.06.006

Balco, G., Stone, J. O., Lifton, N. A., & Dunai, T. J. (2007). A complete and easily accessible means of calculating surface exposure ages or erosion rates from 10be and 26al measurements. *Quaternary Geochronology*, *3*, 174–195. https://doi.org/10.1016/j.quageo.2007.12.001

Basu, A., & Aydin, A. (2004). A method for normalization of schmidt hammer rebound values. *International Journal of Rock Mechanics & Mining Sciences*, *41*, 1211–1214. https://doi.org/10.1016/j.ijrmms.2004.05.001

Bland, W. J., & Rolls, D. (2016). *Weathering: An introduction to the scientific principles.* Routledge.

Blikra, L., Longva, O., Braathen, A., Anda, E., Dehls, J., & Stalsberg, K. (2006). Rock slope failures in norwegian fjord areas: Examples, spatial distribution and temporal pattern. *Landslides from Massive Rock Slope Failure*, *49*, 457–496. https://doi.org/10.1007/978-1-4020-4037-5_26

Castañeda, A., Corvo, F., Howland, J. J., Marrero, R., & Fernandez, D. (2017). Atmospheric corrosion of steel - reinforced concrete in coastal city located on a

tropical island. *Reinforced Concrete: Design, Performance and Applications, New York: Nova Science Publishers*, 109–156.

Då, L. (2020). *Skredkartlegging og -kronologi mellom indreeide og korsmyra, korsmyrdalen, indre sunnmøre* [Master's thesis, Universitetet i Bergen].

Dorren, L. K. A. (2003). A review of rockfall mechanics andmodelling approaches. *Progress in Physical Geography, 27, 1*, 69–87. https://doi.org/10.1191/0309133303pp359ra

Evans, S. G., & Hungr, O. (1993). The assessment of rockfall hazard at the base of talus slopes. *Canadian Geotechnical Journal, 30*, 620–636. https://doi.org/10.1139/t93-054

Ffoulkes, C., & Harrison, S. (2014). Evaluating the schmidt hammer as a method for distinguishing the relative age of late holocene moraines: Svellnosbreen, jotunheimen, norway. *Geografiska Annaler: Series A, Physical Geography, 96:3*, 393–402. https://doi.org/10.1111/geoa.12055

Furseth, A. (2006). *Skredulykker i norge*. Tun Forlag.

Goudie, A. S. (2006). The schmidt hammer ingeomorphological research. *Progress in Physical Geography, 30, 6*, 703–718. https://doi.org/10.1177/0309133306071954

Haldar, S. K. (2020). Quartzite. *Introduction to Mineralogy and Petrology (Second Edition)*, 269–289. https://doi.org/10.1016/b978-0-12-820585-3.00007-7Œ

Hermanns, R., Niedermann, S., Garcia, A. V., & Schellenberger, A. (2006). Rock avalanching in the nw argentine andes as a result of complex interactions of lithologic, structural and topographic boundary conditions, climate change and active tectonics: Landslides from massive rock slope failure. *NATO Science Series IV, 49*, 539–569. https://doi.org/10.1007/978-1-4020-4037-5_27

Hermanns, R., Penna, I. M., Oppikofer, T., Noël, F., & Velardi, G. (2022). Rock avalanche. *Treatrise on Geomorphology, 5*, 85–105. https://doi.org/10.1016/B978-0-12-818234-5.00183-8.

Hermanns, R. L., Schleier, M., Martina Böhme, L. H. B., Gosse, J., Ivy-Ochs, S., & Hilger, P. (2017). Rock-avalanche activity in w and s norway peaks after the retreat of the scandinavian ice sheet. *Advancing Culture of Living with Landslides*, 331–338. https://doi.org/10.1007/978-3-319-53483-1_39

Hilger, P., Hermanns, R. L., Czekirda, J., Myhra, K. S., Gosse, J. C., & Etzelmüller, B. (2021). Permafrost as a first order control on long-term rock-slope deformation in (sub-)arctic norway. *Quaternary Science Reviews*, *251*, 106718. https://doi.org/10.1016/j.quascirev.2020.106718

Hilger, P., Hermanns, R., & Etzelmüller, B. (2022). Fjellskredaktivitet i norge siden den siste istida. *Idunn*, *146*, 94–106. https://doi.org/10.18261/naturen.146.2-3.4

Hilger, P., Hermanns, R. L., Gosse, J. C., Jacobs, B., Etzelmüller, B., & Krautblatter, M. (2018). Multiple rock-slope failures from mannen in romsdal valley, western norway, revealed from quaternary geological mapping and 10be exposure dating. *The Holocene*, *28(12)*, 1841–1854. https://doi.org/10.1177/0959683618798165

Hobber, S. S., & Robbestad, S. H. (2022). *Geologisk kartlegging av fjellskredet ved vardahaugen, lærdalen* [Master's thesis, Høgskulen på Vestlandet].

Hughes, A. L. C., Gyllencreutz, R., Lohne, Ø. S., Mangerud, J., & Svendsen, J. I. (2015). The last eurasian ice sheets – a chronological database and time-slice reconstruction, dated-1. *Boreas*, *45*, 1–45. https://doi.org/10.1111/bor.12142

King, A. P., & Eckersley, R. J. (2019). Inferential statistics iv: Choosing a hypothesis test. *Statistics for Biomedical Engineers and Scientists*, 147–171. https://doi.org/10.1016/b978-0-08-102939-8.00016-5

Kos, A., Amann, F., Strozzi, T., Delaloye, R., von Ruette, J., & Springman, S. (2016). Contemporary glacier retreat triggers a rapid landslide response, great aletsch glacier, switzerland. *Geophysical Research Letters*, *43*, 12 466–12 474. https://doi.org/10.1002/2016GL071708

Løvås, G. G. (2018). *Statistikk for universiteter og høgskoler (4. utgave)*. Universitetsforlaget.

Mangerud, J. (2024). *Yngre dryas* [Last modified January 22, 2024]. Retrieved 18th May 2024, from https://snl.no/yngre_dryas

Marr, P., Winkler, S., & Löffler, J. (2019). Schmidt-hammer exposure-age dating (shd) performed on periglacial and related landforms in opplendskedalen, geirangerfjellet, norway: Implications for mid- and late-holocene climate variability. *The Holocene*, *29*, 97–109. https://doi.org/10.1177/095968361880463

Matthews, J. A., Haselberger, S., Hill, J. L., Owen, G., Winkler, S., Hiemstra, J. F., & Hallang, H. (2020a). Snow-avalanche boulder fans in jotunheimen, southern norway: Schmidt-hammer exposure-age dating, geomorphometrics, dynamics and evolution. *Geografiska Annaler: Series A, Phyical Geography, 102.* https://doi.org/10.1080/04353676.2020.1762365

Matthews, J. A., McEwen, L. J., & Owen, G. (2015). Schmidt-hammer exposure-age dating (shd) of snow-avalanche impact ramparts in southern norway: Approaches, results and implications for landform age, dynamics and development. *Earth Surf. Process. Landforms, 40,* 1705–1718. https://doi.org/10.1002/esp.3746

Matthews, J. A., & Owen, G. (2010). Schmidt hammer exposure-age dating: Developing linear age-calibration curves using holocene bedrock surfaces from the jotunheimen–jostedalsbreen regions of southern norway. *Boreas, 39,* 105–115. https://doi.org/10.1111/j.1502-3885.2009.00107.x

Matthews, J. A., & Wilson, P. (2015). Improved schmidt-hammer exposure ages for active and relict pronival ramparts in southern norway, and their palaeoenvironmental implications. *Geomorphology, 246,* 7–21. https://doi.org/10.1016/j.geomorph.2015.06.002

Matthews, J. A., Wilson, R., & Mourne, R. W. (2017). Landform transitions from pronival ramparts to moraines and rock glaciers: A case study from the smørbotn cirque, romsdalsalpane, southern norway. *Geografiska Annalaler: Series A, Physical Geography, 99(1),* 15–37. https://doi.org/10.1080/04353676.2016.1256582

Matthews, J. A., Winkler, S., Wilson, P., Tomkins, M. D., Dortch, J. M., Mourne, R. W., Hill, J. L., Owen, G., & Vater, A. E. (2018). Small rock-slope failures conditioned by holocene permafrost degradation: A new approach and conceptual model based on schmidt-hammer exposure-age dating, jotunheimen, southern norway. *Boreas, 47,* 144–1169. https://doi.org/10.1111/bor.12336

Matthews, J. A., & McEwen, L. J. (2013). High-precision schmidt-hammer exposure-age dating of flood berms, vetlestølsdalen, alpine southern norway: First application and some methodological issues. *Geografiska Annaler: Series A, Physical Geography, 95:2,* 185–195. https://doi.org/10.1111/geoa.12009

Matthews, J. A., McEwen, L. J., Owen, G., & Los, S. (2020b). Holocene alluvial fan evolution, schmidt-hammer exposure-age dating and paraglacial debris floods in the se jostedalsbreen region, southern norway. *Boreas*, *49*, 886–904. https://doi.org/10.1111/bor.12456

Matthews, J. A., & Shakesby, R. A. (1984). The status of the 'little ice age' in southern norway: Relative-age dating of neoglacial moraines with schmidt hammer and lichenometry. *Boreas*, *13*, 333–346. https://doi.org/10.1111/j.1502-3885.1984.tb01128.x

Matthews, J. A., Wilson, P., Winkler, S., Mourne, R. W., Hill, J. L., Owen, G., Hiemstra, J. F., Hallang, H., & Geary, A. P. (2019). Age and development of active cryoplanation terraces in the alpine permafrost zone at svartkampan, jotunheimen, southern norway. *Quartenary research*, *92*, 641–664. https://doi.org/10.1017/qua.2019.41

Matthews, J. A., & Winkler, S. (2010). Schmidt-hammer exposure-age dating (shd): Application to early holocene moraines and a reappraisal of the reliability of terrestrial cosmogenic-nuclide dating (tcnd) at austanbotnbreen, jotunheimen, norway. *Boreas*, *40*, 256–270. https://doi.org/10.1111/j.1502-3885.2010.00178.x

Matthews, J. A., & Winkler, S. (2011). Schmidt-hammer exposure-age dating (shd): Application to earlyholocene moraines and a reappraisal of the reliability of terrestrialcosmogenic-nuclide dating (tcnd) at austanbotnbreen,jotunheimen, norway. *Boreas*, *40*, 256–270. https://doi.org/10.1111/j.1502-3885.2010.00178.x

Matthews, J. A., & Winkler, S. (2021). Schmidt-hammer exposure-age dating: A review of principles and practice. *Earth-science reviews*, *230, 104038*. https://doi.org/10.1016/j.earscirev.2022.104038Œ

Matthews, J. A., Winkler, S., & Wilson, P. (2014). Age and origin of ice-cored moraines in jotunheimen and breheimen, southern norway: Insights from schmidt-hammer exposure-age dating. *Geografiska Annaler: Series A, Physical Geography*, *96*, 531–548. https://doi.org/10.1111/geoa.12046

McEwen, L. J., Matthews, J. A., & Owen, G. (2020). Development of a holocene glacier-fed composite alluvial fan based on surface exposure-age dating tech-

niques: The illåe fan, jotunheimen, norway. *Geomorphology*, *363*, 107200. https://doi.org/10.1016/j.geomorph.2020.107200

Nesje, A., Blikra, L. H., & Anda, E. (1994). Dating rockfall-avalanche deposits from degree of rock-surface weathering by schmidt-hammer tests: A study from norangsdalen, sunnmøre, norway. *Norsk Geologisk Tidsskrift*, *74*, 108–113.

Nesje, A., Matthews, J. A., Linge, H., Bredal, M., Wilson, P., & Winkler, S. (2020). New evidence for active talus-foot rock glaciers at øyberget, southern norway, and their development during the holocene. *The Holocene*, *31*, 1786–1796. https://doi.org/doi.org/10.1177/09596836211033226

Noël, F., Nordang, S. F., Jaboyedoff, M., Travelletti, J., Matasci, B., Digout, M., Derron, M.-H., Caviezel, A., Hibert, C., Toe, D., Talib, M., Wyser, E., Bourrier, F., Toussaint, R., Malet, J.-P., & Locat, J. (2023). Highly energetic rockfalls: Back analysis of the 2015 event from the mel de la niva, switzerland. *Landslides*, *20*, 1561–1582. https://doi.org/10.1007/s10346-023-02054-2

NVE. (n.d.). *Mannen*. Retrieved 2nd April 2024, from https://www.nve.no/naturfare/overvaking-og-varsling/fjellskredovervaaking/kontinuerlig-overvaakede-fjellpartier/mannen/

Oppikofer, T., Saintot, A., Hermanns, R., Böhme, M., Scheiber, T., Gosse, J., & Dreiås, G. (2017). From incipient slope instability through slope deformation to catastrophic failure — different stages of failure development on the ivasnasen and vollan rock slopes (western norway). *Geomorphology*, *289*, 96–116. https://doi.org/10.1016/j.geomorph.2017.03.015

Ørjaseter, E. (2020). Steinskred i romsdalen natt til fredag. *Åndalsnes avis*. Retrieved 3rd April 2024, from https://www.andalsnes-avis.no/nyheter/i/qRABgz/steinskred-i-romsdalen-natt-til-fredag

Owen, G., Matthews, J. A., & Albert, P. G. (2007). Rates of holocene chemical weathering,'little ice age' glacial erosion andimplications for schmidt-hammer datingat a glacier–foreland boundary,fåbergstølsbreen, southern norway. *The Holocene*, *17,6*, 829–834. https://doi.org/10.1177/0959683607081419

Penna, I. M., Magnin, F., Nicolet, P., Etzelmüller, B., Hermanns, R., Böhme, M., Kristensen, L., Nöel, F., Bredal, M., & Dehls, J. (2023). Permafrost controls the displacement rates of large unstable rock-slopes in subarctic environ-

ments. *Global and Planetary change, 220*, 104017. https://doi.org/10.1016/j.gloplacha.2022.104017

Penna, I., Nicolet, P., Hermanns, R., Böhme, M., & Nöel, F. (2022). *Preliminary inventory of rock avalanche deposits and their related sources in norway. regional distribution, main features and topographic constraints.* Geological Survey of Norway.

Proceq. (2002). *Concrete test hammer.*

Raade, G., & Fossen, H. (2020). *Gneis* [Last modified December 10, 2020]. Retrieved 10th May 2024, from https://snl.no/gneis

Ramberg, I. B., Bryhni, I., Nøttvedt, A., & Rangnes, K. (2013). *Landet blir til.* Norsk Geologisk Forening, Andre utgave.

Romundset, A., Akçar, N., Fredin, O., Andersen, J. L., Høgaas, F., Christl, M., Yesilyurt, S., & Schlüchter, C. (2023). Early holocene thinning and final demise of the scandinavian ice sheet across the main drainage divide of southern norway. *Quaternary Science Reviews, 317*, 108274. https://doi.org/10.1016/j.quascirev.2023.108274.

Sandøy, G., Oppikofer, T., & Nilsen, B. (2016). Why did the 1756 tjellefonna rockslide occur? a back-analysis of the largest historic rockslide in norway. *Geomorphology.* https://doi.org/10.1016/j.geomorph.2016.08.016

Schleier, M., Hermanns, R. L., Gosse, J. C., Oppikofer, T., Rohn, J., & Tønnesen, J. F. (2017). Subaqueous rock-avalanche deposits exposed by post-glacial isostatic rebound, innfjorddalen, western norway. *Geomorphology, 289*, 117–133. https://doi.org/10.1016/j.geomorph.2016.08.024

Schleier, M., Hermanns, R. L., Rohn, J., & Gosse, J. C. (2015). Diagnostic characteristics and paleodynamics of supraglacial rock avalanches, innerdalen, western norway. *Geomorphology, 245*, 23–39. https://doi.org/10.1016/j.geomorph.2015.04.033

Shakesby, R. A., Matthews, J. A., Karlén, W., & Los, S. O. (2011). The schmidt hammer as a holocene calibrated-age dating technique:testing the form of the r-value–age relationship and defining the predicted-age errors. *Sage, The Holocene 21(4)*, 615–628. https://doi.org/10.1177/0959683610391322

Shakesby, R. A., Matthews, J. A., & Owen, G. (2006). The schmidt hammer as a relative-age dating tool and its potential for calibrated-age dating in holocene glaciated environments. *Elsevier*, *25*, 2846–2867. https://doi.org/10.1016/j.quascirev.2006.07.011.

Stahl, T., Winkler, S., Quigley, M., Bebbington, M., Duffy, B., & Duke, D. (2013). Schmidt hammer exposure-age dating (shd) of late quaternary fluvial terraces in new zealand. *Earth Surf. Process. Landforms*, *38*, 1838–1850. https://doi.org/10.1002/esp.3427

Tomkins, M. D., Dortch, J. M., Hughes, P. D., Huck, J. J., Stimson, A. G., Delmas, M., & Pallàs, R. (2018). Rapid age assessment of glacial landforms in the pyrenees using schmidt hammer exposure dating (shed). *Quartenary Research*, *90(1)*, 26–37. https://doi.org/doi:10.1017/qua.2018.12

Tomkins, M. D., Huck, J. J., Dortch, J. M., Hughes, P. D., Kirbride, M. P., & Barr, I. D. (2017). Schmidt hammer exposure dating (shed): Calibration procedures, new exposure age data and an online calculator. *Elsevier*, *Quaternary Geochronology 44*, 55–62. https://doi.org/10.1016/j.quageo.2017.12.003

Walker, M. (2005). *Quartenary dating methods*. Wiley.

Wilson, P., Linge, H., Matthews, J. A., Mourne, R. W., & Olsen, J. (2019). Comparative numerical surface exposureage dating (10be and schmidt hammer) of an early-holocene rock avalanche at alstadfjellet, valldalen, southern norway. *Geografiska Annaler: Series A, Physical Geography*, *101:4*, 293–309. https://doi.org/10.1080/04353676.2019.1644815

Winkler, S., Matthews, J. A., Mourne, R. W., & Wilson, P. (2016). Schmidt-hammer exposure ages from periglacial patterned ground (sorted circles) in jotunheimen, norway, and their interpretative problems. *Geografiska Annaler: Series A, Physical Geography*, *98:3*, 265–285. https://doi.org/10.1111/geoa.12134

Zasadni, J., & Kłapyta, P. (2016). From valley to marginal glaciation in alpinetype relief: Lateglacial glacier advances in the pieć stawów polskich/roztoka valley, high tatra mountains, poland. *Geomorphology*, *253*, 406–424. https://doi.org/10.1016/j.geomorph.2015.10.032

Appendix

A Coordinates and dating technique for calibration sites

Granitic ortogneiss/migmatic gneiss

Number	Site	Coordinates	Dating technique
1	Alstadfjellet	62.329285, 7.488482	10Be
2	Gråfonnfjellet old	62.463670, 7.505385	10Be
3	Gråfonnfjellet middle	62.459726, 7.512778	10Be
4	Gråfonnfjellet young	62.457117, 7.508820	10Be
5	Gråura	62.566158, 7.521030	10Be
6	Venja	62.519783, 7.769456	14C
11	Svarttinden	62.413456, 7.853133	10Be
12	Mongefossen	62.438741, 7.883377	Historical
13	Skiri	62.429755, 7.954492	10Be
20	Ivasnasen	62.565276, 9.124890	10Be

Granitic gneiss/granite

Number	Site	Coordinates	Dating technique
14	Setra, Eikesdalen	62.447402, 8.275388	10Be
15	Hølsteingjerdet, Eikesdalen	62.459873, 8.216790	10Be
16	Tjellefonna	62.765091, 7.874207	Historical
17	Hanging moraine, Innerdalen	62.738175, 8.726088	10Be
18	Innerdalsvatnet	62.728080, 8.736960	10Be
19	Fluotjønna, Innerdalen	62.719222, 8.756879	10Be

Silimanitic gneiss

Number	Site	Coordinates	Dating technique
7	Mann23	62.466354, 7.793283	10Be
8	Mann31	62.466730, 7.791460	10Be
9	Mann36	62.467655, 7.789855	10Be
10	Mann38	62.469215, 7.788826	10Be

Table 9: Locations and dating techniques used to determine age for the calibration sites

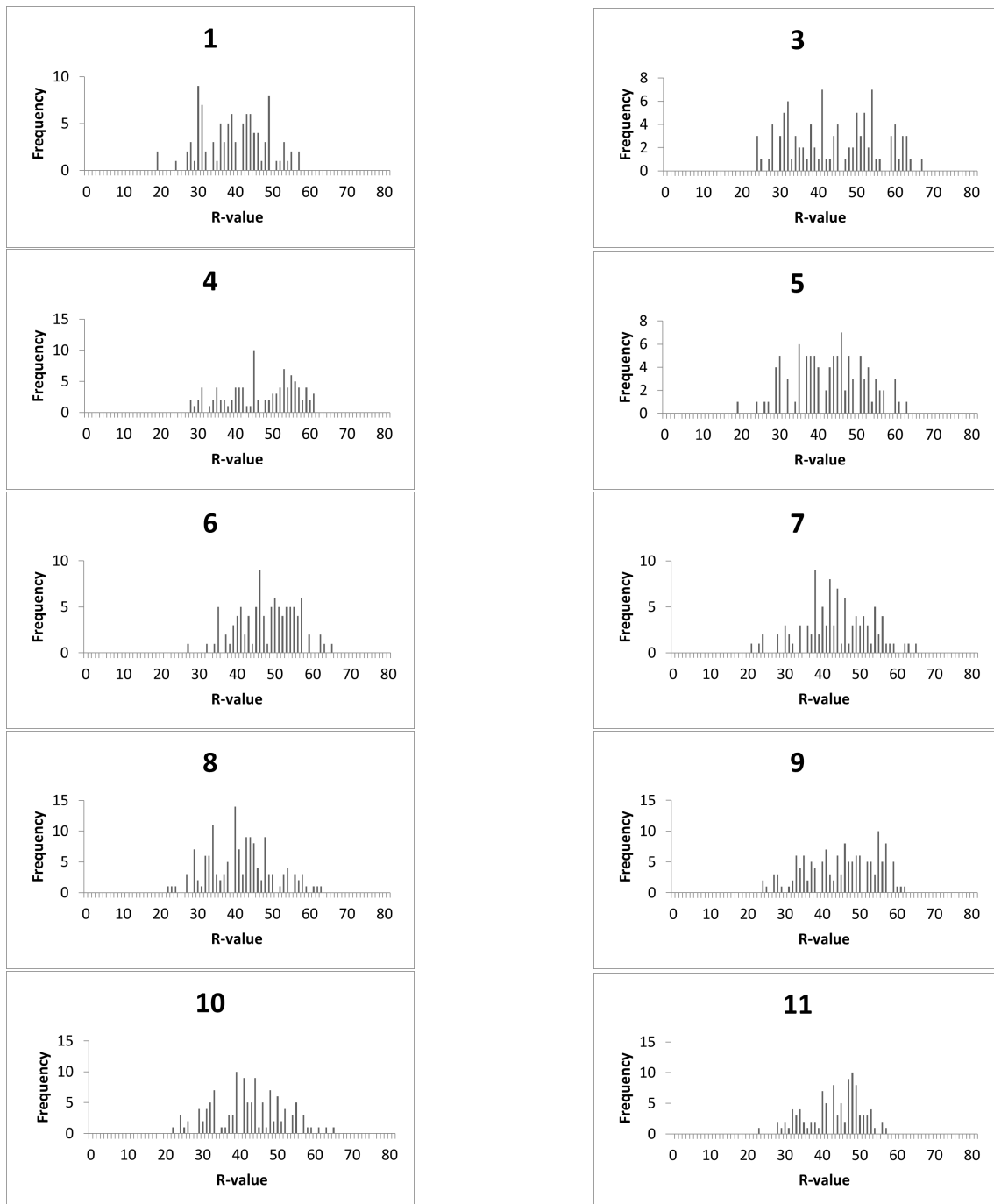# B   Histograms for calibration sites

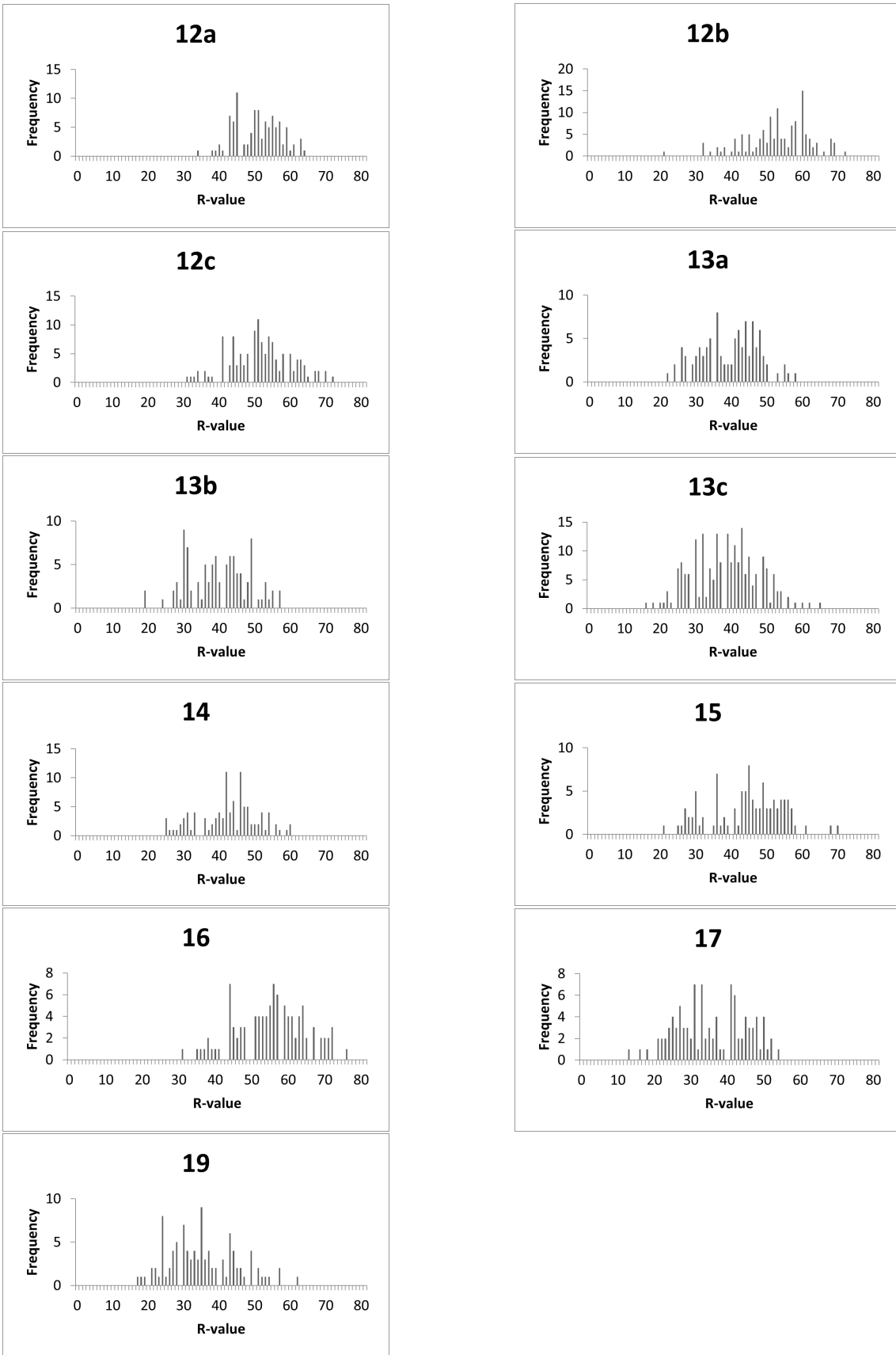Figure 37: Histograms for the different calibration sites 1-11

Figure 38: Histograms for the different calibration sites 12a-19

C Data from ^{14}C-dating of tree found under rock at Gråfonnfjellet

Sample Name	TRa-22693	14C content (pMC)	14C Age (rounded)	d13C (AMS system)
TRa-22693	Salix sp., Alkali residue	95.68 ± 0.14	355 ± 10	-23.9 ± 0.2 ‰

Calibrated Age Ranges	% C	mgC	Fraction Yield(%)	14C Age (not rounded)
68.3% probability				
1484AD (34.6%) 1515AD				
1591AD (33.6%) 1620AD	48	1,74	74	355 + 12/-12 BP
95.4% probability				
1473AD (46.5%) 1524AD				
1572AD (48.9%) 1631AD				

Table 10: Results from the radiocarbon dating of a tree found under a large boulder.

D Statistical parameters

Calibration sites

Site	1	2	3	4	5	6	7	8
Mean (Calibrated)	39.2	45.1	46.3	43.7	42.6	47.1	41.7	44.5
Median (Calibrated)	39.3	47.8	47.0	43.5	43.3	48.2	41.1	45.6
STD	8.6	8.9	9.0	11.5	9.3	7.3	9.3	9.4
Mean R2-R1	11.6	6.6	6.4	7.8	8.05	5.23	8.12	-
Anvil mean	72.1	79.1	79.3	79.3	71.3	80.7	75.8	82.0
Anvil STD	2.0	1.2	0.7	0.7	1.8	0.6	1.6	0.3

Site	9	10	11	12a	12b	12c	13a	13b
Mean (Calibrated)	41.0	43.2	43.0	50.4	52.5	51.1	39.0	40.9
Median (Calibrated)	40.2	43.0	44.7	50.2	52.7	50.7	40.3	41.0
STD	8.7	9.0	7.5	6.3	9.1	8.6	8.0	8.2
Mean R2-R1	-	-	7.81	4.71	-	-	10.35	10.45
Anvil mean	74.6	74.6	79.7	79.3	76.8	72.7	79.4	71.1
Anvil STD	1.4	1.5	0.5	0.8	1.8	1.7	1.6	1.9

Site	13c	14	15	16	17	18	19	20
Mean (Calibrated)	38.0	42.1	43.7	54.7	51.3	35.1	34.8	46.9
Median (Calibrated)	38.0	42.3	44.1	55.8	51.5	34.8	34.8	47.0
STD	9.1	8.3	9.9	9.6	9.8	9.5	9.7	10.6
Mean R2-R1	-	-	-	4.71	-	-	-	-
Anvil mean	72.5	79.0	79.2	72.1	79.2	79.4	79.4	71.2
Anvil STD	1.8	1.9	0.8	1.9	0.9	1.8	1.8	1.7

Undated sites

Site	A	B	C	D	E	F	G
Mean (Calibrated)	39.2	40.6	39.4	42.3	40.6	40.7	41.6
Median (Calibrated)	39.3	39.9	39.5	41.0	41.2	40.9	41.4
STD	7.2	9.2	9.1	7.2	7.4	9.5	8.8
Anvil mean	71.1	77.1	81.9	71.1	74.7	78.2	73.3
Anvil STD	1.9	1.0	0.7	1.8	1.0	1.2	0.8

Table 11: Statistical parameters. Numbering according to figure 13